Received: 19 March 2024 | Revised: 19 July 2024 | Accepted: 25 July 2024

DOI: 10.1111/jnc.16199

Journal of Neurochemistry JNC The Official Journal of the International Society for Neurochemistry WILEY

ORIGINAL ARTICLE

Targeting the PAC1 receptor mitigates degradation of myelin and synaptic markers and diminishes locomotor deficits in the cuprizone demyelination model

Margo I. Jansen[1] | Yasir Mahmood[1] | Jordan Lee[1] | Sarah Thomas Broome[2] | James A. Waschek[2] | Alessandro Castorina[1]

[1]Laboratory of Cellular and Molecular Neuroscience, School of Life Sciences, Faculty of Science, University of Technology Sydney, Sydney, New South Wales, Australia

[2]Semel Institute for Neuroscience and Human Behavior/Neuropsychiatric Institute, Intellectual and Developmental Disabilities Research Center, University of California, Los Angeles, Los Angeles, California, USA

Correspondence
Alessandro Castorina, Laboratory of Cellular and Molecular Neuroscience, School of Life Sciences, Faculty of Science, University of Technology Sydney, Sydney, NSW 2007, Australia.
Email: alessandro.castorina@uts.edu.au

Funding information
Rebecca L. Cooper Medical Research Foundation, Grant/Award Number: PG2020710

Abstract

Multiple sclerosis (MS) is a demyelinating disease of the central nervous system with a strong neuroinflammatory component. Current treatments principally target the immune system but fail to preserve long-term myelin health and do not prevent neurological decline. Studies over the past two decades have shown that the structurally related neuropeptides VIP and PACAP (vasoactive intestinal peptide and pituitary adenylate cyclase-activating polypeptide, respectively) exhibit pronounced anti-inflammatory activities and reduce clinical symptoms in MS disease models, largely via actions on their bivalent VIP receptor type 1 and 2. Here, using the cuprizone demyelination model, we demonstrate that PACAP and VIP, and strikingly the PACAP-selective receptor PAC1 agonist maxadilan, prevented locomotor deficits in the horizontal ladder and open field tests. Moreover, only PACAP and maxadilan were able to prevent myelin deterioration, as assessed by a reduction in the expression of the myelin markers proteolipid protein 1, oligodendrocyte transcription factor 2, quaking-7 (APC) and Luxol Fast Blue staining. Furthermore, PACAP and maxadilan (but not VIP), prevented striatal synaptic loss and diminished astrocyte and microglial activation in the corpus callosum of cuprizone-fed mice. In vitro, PACAP or maxadilan prevented lipopolysaccharide (LPS)-induced polarisation of primary astrocytes at 12–24 h, an effect that was not seen with maxadilan in LPS-stimulated microglia. Taken together, our data demonstrates for the first time that PAC1 agonists provide distinctive protective effects against white matter deterioration, neuroinflammation and consequent locomotor dysfunctions in the cuprizone model. The results indicate that targeting the PAC1 receptor may provide a path to treat myelin-related diseases in humans.

KEYWORDS
demyelination, maxadilan, multiple sclerosis, neuroinflammation, pituitary adenylate cyclase-activating polypeptide, vasoactive intestinal polypeptide

Abbreviations: CC1, adenomatous polyposis coli; CNS, central nervous system; EAE, experimental autoimmune encephalomyelitis; GFAP, glial fibrillary acidic protein; IBA1, ionised calcium-binding adapter molecule 1; MBP, myelin basic protein; MOG, myelin oligodendrocyte protein; MS, multiple sclerosis; Olig2, oligodendrocyte transcription factor 2; PAC1, pituitary adenylate cyclase-activating receptor 1; PACAP, pituitary-adenylate cyclase-activating polypeptide; PLP1, proteolipid protein 1; RRID, Research Resource Identifier; SYP, Synaptophysin; VIP, vasoactive intestinal polypeptide; VPAC1, vasoactive intestinal polypeptide receptor 1; VPAC2, vasoactive intestinal polypeptide receptor 2.

1 | INTRODUCTION

Multiple sclerosis (MS) is a chronic neuroinflammatory and demyelinating disease characterised by the appearance of multifocal lesions in the central nervous system (CNS) white matter, peripheral immune cell infiltration and subsequent axonal degeneration (Compston & Coles, 2008). The aetiology of MS is unknown; however, both genetic and environmental factors play a significant role in disease onset and progression (Mechelli et al., 2010). Demyelination and inflammation go hand in hand in MS pathogenesis, being two main factors contributing to the exacerbation of the condition. Currently, the most widely stated hypothesis of MS aetiology maintains that the infiltration of autoreactive peripheral immune cells into the CNS is the primary pathological event to initiate the disease. In this context, the invasion of immune cells into the CNS drives demyelination, followed by oligodendrocyte cell loss, gliosis and finally neurodegeneration (Compston & Coles, 2008). However, there is controversy around whether neuroinflammation, in fact, initiates the MS pathogenic cascade or if it is secondary to the initial oligodendrocyte cell death and myelin loss (Barnett & Prineas, 2004; Lubetzki & Stankoff, 2014; Lucchinetti et al., 2000).

Irrespective of its temporal involvement in MS pathogenesis, chronic neuroinflammation remains a critical hallmark of the disease, especially during relapses. In fact, persistent inflammation limits the ability of the CNS to spontaneously regenerate damaged myelin and inhibits glial and neuronal survival mechanisms (Franklin & Simons, 2022). At present, there is no cure for MS. Currently available disease-modifying treatments (DMTs) target the peripheral immune system and treated patients are subject to adverse effects due to the immunosuppressive functions (Dargahi et al., 2017; Gajofatto & Benedetti, 2015; Hauser & Cree, 2020). Efforts to developing drugs able to preserve myelin integrity and promote remyelination are underway; however, none of these drugs have, as yet, made it past phase II clinical trials (Cunniffe & Coles, 2021; Mi et al., 2013). Therefore, it is important to identify new potential DMTs able to preserve myelin health.

Pituitary-adenylate cyclase-activating polypeptide (PACAP) and vasoactive intestinal polypeptide (VIP) neuropeptides are known for their broad anti-inflammatory and neuroprotective properties (Abad & Waschek, 2011; Jansen et al., 2022; Waschek, 2013). Three heterotrimeric G-protein-coupled receptors are known to mediate the actions of these peptides. Pituitary adenylate cyclase-activating receptor 1 (PAC1) interacts only with PACAP with high affinity, whereas vasoactive intestinal polypeptide receptor 1 (VPAC1) and vasoactive intestinal polypeptide receptor 2 (VPAC2) can interact with either VIP or PACAP with high affinity. By taking advantage of the experimental autoimmune encephalomyelitis (EAE) mouse model of MS, researchers have started exploring the role of the PACAP/VIP system as a treatment strategy to halt the development and progression of MS, highlighting the potential therapeutic application of these neuropeptides (Abad & Waschek, 2011; Jansen et al., 2022; Tan & Waschek, 2011). In addition, evidence from PACAP-deficient mice showed worsened clinical course and increased mortality rate in the EAE model (Tan et al., 2013). In vitro studies demonstrated that PACAP and VIP exhibit anti-inflammatory activities on microglia cells, the resident immune cells of the CNS and can stimulate myelin-related proteins and prevent apoptosis in schwannoma cells (Castorina et al., 2008, 2014; Karunia et al., 2021).

Whilst results with the EAE model have provided essential clues on the immune modulatory effects of these neuropeptides, this preclinical model does not address certain pathogenic mechanisms of demyelination, such as whether these endogenous molecules can prevent myelin loss, as observed in the CNS of MS patients (Ransohoff, 2012) Therefore, alternative preclinical models addressing these pathogenic features should be utilised to investigate this aspect of the disease. One such model is the cuprizone intoxication model of demyelination (Praet et al., 2014). This animal model takes advantage of the demyelinating properties of the copper-chelator cuprizone (administered via the diet) to create a reversible demyelination associated with a secondary neuroinflammatory response in the CNS at sites of damage (white matter) within 4 weeks of treatment (Yamanaka et al., 2023; Zhang et al., 2019). Cuprizone fed mice usually develop locomotor deficits and myelin loss, mimicking several behavioural and molecular features of MS pathology (Franco-Pons et al., 2007; Ghaiad et al., 2017; Lerner et al., 2007).

In this study, we aimed to investigate—for the first time—if targeting the PAC1 receptor could prevent white matter gliosis and preserve myelin integrity and associated locomotor deficits in the cuprizone model of MS. In addition, we performed in vitro experiments in isolated primary astrocytes or microglia challenged with lipopolysaccharide (LPS) to determine the relative contribution of PAC1 receptors to the anti-inflammatory properties elicited by the neuropeptides in each glial cell population.

2 | MATERIALS AND METHODS

2.1 | Animals

Fifty-six male C57BL/6 mice (7-week-old) weighing approximately ~20 g were purchased from the Animal Resources Centre (ARC; Perth, WA, Australia; RRID:IMSR_JAX:000664). Upon arrival, mice were allowed to acclimatise for 1 week prior to the experimental protocol and were then divided into five treatment groups: (1) Standard chow + saline intraperitoneal [i.p.], (2) cuprizone (CPZ) diet + saline i.p., (3) CPZ + PACAP, (4) CPZ + VIP and (5) CPZ + Maxadilan ($n = 12$/group; Figure 1a). Mice were housed in individually ventilated cages (4 mice/cage) under a 12 h light/dark cycle, with access to food and water ad libitum. All experiments were carried out with the approval of the University of Technology Sydney (ETH17-1991) and conducted in compliance with the Australian Code of Practice for the Care and Use of Animals for Scientific Purposes.

2.2 | Experimental protocol

The experimental protocol involved feeding mice either a standard chow or a diet supplemented with 0.2% CPZ for 28 days ($n = 10–12$/group; Figure 1b). Group size was based on results obtained in previous studies using the same demyelination model (Liebetanz & Merkler, 2006; Liu et al., 2010; Matsushima & Morell, 2001), and $n = 10–12$ mice was estimated as the most suitable number of animals to assign to each group to obtain sufficient statistical power, confirmed by a priori calculations ($1-\beta = 0.8–0.9$) with alpha levels set at 0.05. No randomisation was performed to allocate animals in the study and no inclusion/exclusion criteria were applied in the experimental design. However, a weight loss > 15% was set as the limit for inclusion, based on ethical reasons, but none of the animals ever reached the weight limit. CPZ diet was prepared daily by mixing standard rodents' pellets (grounded into powder) with 0% (control) or 0.2% CPZ (C9012-25G, Sigma-Aldrich), since previous evidence demonstrated that the addition of CPZ to grounded chow increases microglia and axonal damage in the corpus callosum and guarantees more consistent and reproducible demyelination compared to CPZ in pellets (Hochstrasser et al., 2017). In addition, this approach ensured that food and CPZ were provided fresh every day. Working concentrations of PACAP (Sigma-Aldrich; A1439), VIP (AusPep) and PAC1-agonist Maxadilan trifluoroacetate (Bachem AG) were prepared in sterile saline (Lerner et al., 2007). Every other day, each mouse received either a saline, or PACAP (90.68 ng/kg), VIP (66.52 ng/kg) or Maxadilan (137.32 ng/kg) i.p. in a final volume of 0.1 mL, corresponding to a final dose of 5 nmol/mouse. PACAP and VIP dosages were based on previous work (Delgado et al., 1999), whereas that of maxadilan was based on the similar affinity of both peptides for PAC1 receptors (Lerner et al., 2007). Mice weights were recorded daily to monitor overall well-being. Every 7 days, starting from day 0, mice were assessed for changes in locomotor behaviours. The open field test was used to examine general ambulation and exploratory behaviour (Seibenhener & Wooten, 2015), which is a tool often used to assess locomotor behaviour in vivo (Franco-Pons et al., 2007; Kraeuter et al., 2019; Seibenhener & Wooten, 2015; Tatem et al., 2014). The horizontal ladder test was utilised to assess locomotor coordination (Metz & Whishaw, 2009). On day 29, mice were sacrificed using CO_2 asphyxiation (EA-33000TS SMARTBOX® Prodigy, Total CO_2 3.01 L/min). Pedal plus eye reflexes were checked to verify death of the animal followed by a cardiac bleed. Brains were collected and snap-frozen for molecular analyses or fixed for 24 h in 4% paraformaldehyde (by immersion) for immunohistochemical analyses. No blinding was performed and no tests for outliers were conducted.

2.3 | Horizontal ladder test

To assess locomotor coordination, we utilised the horizontal ladder test, following the protocol described in Metz and Whishaw (2009). The apparatus consists of a plexiglass tunnel of 60 cm equipped with 60 adjustable metal rungs, each with a diameter of 2 mm and 1 cm spacing in-between. The width of the tunnel/ladder was set at 5 cm and elevated to 30 cm above the bench using a neutral cage on one side, and the animal home cage on the other. Mice were allowed to familiarise with the apparatus before the actual testing. For these sessions, rungs were regularly spaced. In contrast, during the testing session, rungs were adjusted in at least five different irregular patterns to prevent mice from learning the rungs arrangements. On the testing day, each animal was allowed to cross the ladder three times in the same direction (from the neutral to the home cage) and each passage was filmed at a lateral angle (30 frames/s). Recorded videos were analysed at a higher frame rate for increased accuracy using VirtualDub (v1.10.4; 50 frames/s). The foot-fault scoring system developed by Metz and Whishaw (2002, 2009) was then applied to determine the correct (or faulty) positioning of both the front- and hind limbs of mice. An average error score was also calculated from the three trials and used for analysis. Additionally, we averaged the time required to complete the ladder test, to which we subtracted the immobility time.

2.4 | Open field test

The open field test was utilised to assess mobility and exploratory behaviour in mice (Kraeuter et al., 2019). Prior to testing, mice were allowed to acclimatise to the behaviour room for 30 min in the dark. Afterwards, mice were placed in a dark grey square Perspex box (40 cm × 40 cm × 50 cm) and allowed to freely explore the open space in the dark for 5 min, whilst being filmed from the top using an infrared video camera (Sony FDRAX53 4K Full HD Handycam, 1/50fps, in the dark) held by a Manfrotto 190X tripod. Location tracking of the footage was performed using ezTrack (3 min/mouse) (Pennington et al., 2019).

2.5 | Real time-quantitative PCR

To assess the effects of experimental treatments on the expression of neuropeptides' receptors, core myelin genes and glial activation markers, the corpus callosum (rich in myelin) was micro-dissected from frozen brains under a stereoscopic microscope (10× magnification) under RNAse-free conditions. Briefly, the brain was removed from the skull by making an incision along the midline using dissecting scissors. Then, it was separated from the skull using fine forceps and placed it in a Petri dish containing cold PBS. Under a dissecting microscope, any remaining meninges or blood vessels attached to the surface of the brain were gently removed. Using a scalpel, the brain was cut coronally at a level corresponding to about +0.5–1.0 mm from Bregma and a second cut was performed at −1.0–1.5 mm, to obtain a block encompassing the callosal structures located above the striatum. The corpus callosum was then carefully separated from the surrounding grey matter using two 23-gauge needles, which were used as scalpels. This approach allowed increased dissection accuracy. Dissected callosal structures (rich in white matter) were then placed in ice-cold PBS and collected for storage/downstream analyses. Total RNA was extracted using TRI-reagent (T9424-200ML, Sigma Aldrich) and precipitated using 2-propanol as previously described (Mandwie et al., 2021). Complementary DNA (cDNA) was generated using the Tetro cDNA Synthesis kit according to manufacturer's instructions

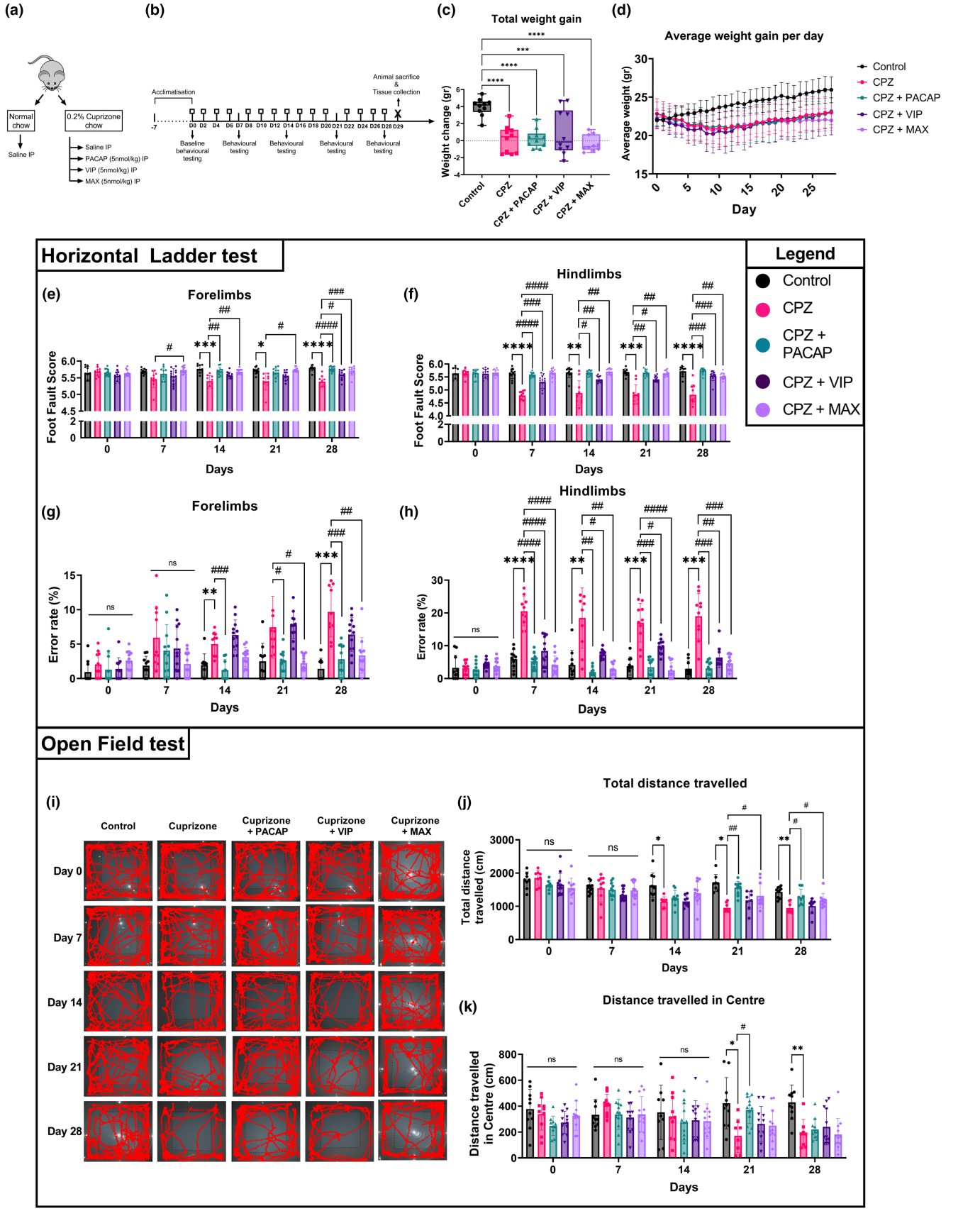

(BIO-65043, Bioline). Each RT-qPCRs reaction contained 5 μL iTaq Universal SYBR Green Supermix (Cat. No. #1725124, Bio-rad), 3 μL of cDNA (100 ng), 0.8 μL forward (500 nM) and reverse primer (500 nM). Ribosomal protein S18 was used as a reference gene. Table 1 illustrates the oligonucleotides sequences of the RT-qPCR optimised primer sets used in this study. For the analysis, relative mean fold

FIGURE 1 Pituitary adenylate cyclase-activating polypeptide (PACAP), vasoactive intestinal peptide (VIP) or Maxadilan treatment prevents the locomotor deficits caused by cuprizone. Schematic overview of (a) the experimental groups and (b) timeline for treatments and behavioural assessments. Squares indicate days in which mice received intraperitoneal peptides' injections. The cuprizone (CPZ) and control diets commenced on day 1 and continued until the day of tissue collection (day 29). (c) Shows the overall weight change in response to diet/treatment. (d) Line graph showing the daily average weight of mice throughout the experimental timeline. Average foot fault scores measured in the (e) forelimbs and (f) hindlimbs of mice. (g) Error rates (shown as %) for the forelimbs and (h) hindlimbs of mice in each group. (i) Representative linetracks showing the trajectory of mice while exploring the open field apparatus. Bar graphs showing the (j) total distance travelled and (k) distance travelled in centre. Statistics in C were computed using one-way ANOVA followed by Sidak's multiple comparison tests, showing significant changes with respect to control $^{***}p < 0.001$ or $^{****}p < 0.0001$. $n = 10–12$ mice per group for weight. Behavioural data was analysed using mixed-effects ANOVA followed by Tukey's multiple comparison's test. Results are the mean ± SD. $^{*}p < 0.05$, $^{**}p < 0.01$, $^{***}p < 0.001$, $^{****}p < 0.0001$ vs. Control. $\#p < 0.05$, $\#\#p < 0.01$, $\#\#\#p < 0.001$, $\#\#\#\#p < 0.0001$ vs. Cuprizone. $n = 10–12$ mice per group.

changes in gene expression were calculated using the ΔΔCt method as described previously (Thomas Broome et al., 2021). Primer specificity was determined by running a melting curve analysis at the end of each PCR amplification.

2.6 | Luxol fast blue staining

Half of the brains from each experimental group were fixed in 4% paraformaldehyde (PFA; 158127-500G, Merck) for 24 h before tissue processing (Excelsior™ AS Tissue Processor) and embedding in paraffin (The Epredia™ HistoStar™ embedding workstation). Serial coronal sections (each 5 μm thick) spanning the antero-posterior extension of the corpus striatum (between +1.0 and −1.5 mm from Bregma) were cut using a microtome (Epredia™ HM 325 microtome) and were collected on silane-coated slides (StarFrost, QLD, Australia). To assess myelin integrity, sections were stained with Luxol Fast Blue (LFB) staining (0.1% LFB in 95% ethanol; S3382-25G, Sigma-Aldrich). To perform this histological evaluation, sections were deparaffinised in xylene (3× 5 min), followed by a 100% ethanol step (2× 5 min) and a 95% ethanol step (5 min) before overnight incubation with LFB staining solution at 58°C. The next day, sections were rinsed in 95% ethanol prior to a brief differentiation step in Lithium Carbonate (0.05% in ddH_2O, 255823-100G, Sigma Aldrich) and a further rinse in 70% ethanol. Afterwards, sections were counterstained using 0.1% Cresyl Violet solution (10 min at RT, C5042-10G, Merck). After a rinse in ddH_2O and a differentiation step in 95% ethanol, slides were dehydrated, mounted using VectaMount Express Mounting medium (H-5700-60, Abacus DX) and cover slipped. Stained sections were imaged using the Zeiss Axioscan Z1 (20×, ZEISS). Images were analysed in ImageJ/FIJI (version 1.53k). Myelin intensity in the corpus callosum was quantified by separating the LFB staining from the Cresyl Violet counterstaining using the colour deconvolution plugin (v2.1) followed by thresholding and measuring the mean grey value.

2.7 | Immunohistochemistry

Serial coronal sections taken at the same antero-posterior coordinates as for LFB staining were deparaffinised in xylene and rehydrated using decreasing concentrations of ethanol to H_2O. Following an antigen-retrieval step of 15 min (10 mM citric acid, 0.05% Tween-20, pH 6.0), Proteolipid protein (PLP) (1:2000, Abcam Cat# ab254363, RRID:AB_3095302), Olig2 (1:200, Cell Signalling Technology Cat# 65915, RRID:AB_2936997) or anti-adenomatous polyposis coli (APC, aka Quaking 7 or CC1) (1:100, Sigma-Aldrich Cat# SAB4501438, RRID:AB_10762093) immunoreactivity was assessed using the Rabbit specific HRP/DAB (ABC) Detection IHC Kit (Abcam Cat# ab64261, RRID:AB_2810213) according to manufacturer's instructions. Haematoxylin (Lillie Mayer's, POCD healthcare) was used to counterstain nuclei. Following this, sections were dehydrated using increasing concentrations of ethanol and xylene and mounted using VectaMount Express Mounting medium (H-5700-60, Abacus DX). Stained sections were imaged using the Zeiss Axioscan Z1 (20×, Carl Zeiss). Images were analysed with ImageJ/FIJI (version 1.53k). The average intensity of DAB staining was measured in at least three selected sections per mouse ($n = 6$ per group) taken along the rostro-caudal axis of the corpus callosum, which were used to assess alterations in white matter PLP and Quaking 7 immunoreactivity. Briefly, following a colour deconvolution step, a universal threshold was set for all images and the mean grey intensity values in the corpus callosum were measured. To measure the number of $Olig2^+$ nuclei, regions of interest ($200 \times 200\,\mu m = 40000\,\mu m^2$) selected from the corpus callosum of each mouse were colour deconvolved. Thereafter, universal threshold was set, and the number of cells and size of nuclei were determined using the particle analysis plug-in of ImageJ/FIJI after a thresholding step. To calculate the average # of cells/mm^2 we applied the following formula:

Cells / (mm^2) = ((average # cells in each ROI × 10^6)) / ROI area.

2.8 | Immunofluorescence

Immunofluorescence staining was performed based on a protocol published by Kajimura et al. (Kajimura et al., 2016) with minor modifications. Briefly, sections were deparaffinised and rehydrated using xylene and decreasing concentrations of ethanol. After an antigen-retrieval step of 15 min (10 mM citric acid, 0.05% Tween-20, pH 6.0), an auto-fluorescence quenching step was performed by submerging the sections in a solution containing 0.25% NH_3 in 70% ethanol for 1 h at RT, followed by a permeabilisation step of 20 min (0.4% Triton-X100 in PBS). A brief hydrogen peroxide step (3% H_2O_2 in methanol, 15 min) was performed to block

TABLE 1 Primer sets used in RT-qPCR analyses.

Accession #	Gene	Primer sequence (5′-3′)	Length (bp)
NM_009625.3	*Adcyap1*	Fwd: GATCAGACCAGAAGACGAGG	129
		Rev: GCTGGATAGTAAAGGGCGTAAG	
NM_011702.3	*Vip*	Fwd: GACCACCTTCTGTAGTGAGTAG	117
		Rev: TTTCTGCTAAGGGATTCTGCAA	
NM_007407.4	*Adcyap1r1*	Fwd: TATCCACCATTACTCTACGGCT	91
		Rev: TCTGGAGAGAAGGCAAATACTG	
NM_011703.4	*Vipr1*	Fwd: CCCTCTGTTTGGAGTTCACTAT	88
		Rev: TACGACGAGTTCAAAGACCATT	
NM_009511.2	*Vipr2*	Fwd: ATTTCATAGATGCGTGTGGCTA	126
		Rev: TGCTTCCTGTTGTAAGAGACAT	
NM_011123.4	*Plp1*	Fwd: ATGCCAGAATGTATGGTGTTCT	200
		Rev: TTTAAGGACGGCGAAGTTGTAAG	
NM_010814.2	*Mog*	Fwd: CTTCTTCAGAGACCACTCTTACC	71
		Rev: CCCAATAGAAGGGATCTTCCAC	
NM_001025251.2	*Mbp*	Fwd: TATAAATCGGCTCACAAGGGATT	85
		Rev: TGTCTCTTCCTCCCAGCTTA	
NM_016967.2	*Olig2*	Fwd: AAAGACAAGAAGCAGATGACTGA	200
		Rev: AGCATGAGGATGTAGTTTCGC	
NM_001361501.1	*Iba1*	Fwd: ACGTTCAGCTACTCTGACTTTC	107
		Rev: GTTGGCCTCTTGTGTTCTTTG	
NM_001131020.1	*Gfap*	Fwd: GAGATTCGCACTCAATACGAGG	79
		Rev: CTGCAAACTTAGACCGATACCA	
NM_011296.2	*S18*	Fwd: CCCTGAGAAGTTCCAGCACA	145
		Rev: GGTGAGGTCGATGTCTGCTT	

endogenous peroxidase activity. Sections were blocked for 1 h in 5% BSA (0.2% gelatin, 0.25% Triton-X100 in PBS). Primary antibody dilutions were prepared in 1% BSA (0.2% gelatin, 0.25% Triton-X100 in PBS) and incubated overnight (4°C). Slides were incubated with secondary antibodies for 1 h at RT in the 1% BSA solution, before being mounted using Vectashield® Antifade Mounting Medium containing DAPI (H-1200-10, Abacus DX). Primary antibodies used for these experiments were Rabbit-anti-GFAP (1:250, Abcam Cat# ab68428, RRID:AB_1209224), Mouse-anti-IBA1 (1:250, GeneTex Cat# GTX632426, RRID:AB_2888314), Rabbit-anti-SYP (1:200, Santa Cruz Biotechnology Cat# sc-9116, RRID:AB_2199007), Mouse-anti-TUJ1 (1:200, BioLegend Cat# 801201 (also 801 202, 801 213), RRID:AB_2313773), Rabbit-anti-NEFL (1:250, Thermo Fisher Scientific Cat# MA5-14981, RRID:AB_10984147), Goat anti-mouse IgG H&L (Alexa Fluor® 594) (1:500, Abcam Cat# ab150116, RRID:AB_2650601) and Goat anti-rabbit IgG (H+L), F(ab')2 Fragment (Alexa Fluor® 488 Conjugate) (1:500, Cell Signalling Technology Cat# 4412 (also 4412S), RRID:AB_1904025). All stained sections were imaged using the Zeiss Axioscan Z1 (20×, Zeiss). Images were analysed in ImageJ/FIJI (version 1.53k). For fluorescence intensity measurements, a universal threshold setting was applied to all images, and the mean intensity of each channel was measured specifically in the corpus callosum and plotted relative to the intensity in control mice. $GFAP^+$ or IBA^+ cell counts in the corpus callosum were measured as described above for $Olig2^+$ nuclei. Figures were generated using OMERO.figure (version 4.2.0).

2.9 | Primary glia cultures & treatments

Primary cultures of astrocytes or microglial cells were prepared as per the protocol described by Piper et al. (2023) and Schildge et al. (2013) with minor modifications. Briefly, whole brains of P0-P2 C57BL/6 mice (ARC; Perth, WA, Australia; RRID:IMSR_JAX:000664) pups were isolated (4–5 pups per prep/three independent repeats) and dissected under sterile conditions using filtered Hanks' balanced salt solution (H9394, Sigma-Aldrich). Cortices were pooled and collected for mixed glia cell isolation. After a trypsin/EDTA digestion (0.25% trypsin/EDTA for 30 min at 37°C; Sigma-Aldrich) and DNase I treatment step (10 mg/mL, Sigma-Aldrich), the cell suspension was centrifuged (300 rpm, 5 min) followed by a triturated step to further dissociate the tissue and obtain a single cell solution. Cells were plated in a T75 flask ($10–15 \times 10^6$ cells) for 10–11 days (or until 80%–90% confluent), with media replacements on alternate days. After 10 days, to isolate microglial cells, the mixed glial cultures were placed on an oscillator (200 rpm × 2 h, RT). Supernatants containing enriched microglia were then centrifuged at 1200 rpm × 5 min and plated on

poly-D-Lysine-coated (PDL; P6407, Sigma-Aldrich; diluted in milliQ H_2O) glass ViewPlate 96-well plates for immunocytochemistry (PerkinElmer). The remaining culture consisting of astrocytes and OPCs was further dissociated using an oscillator (240 rpm × 4 h, RT), followed by vigorous tapping for 1 min to remove any residual OPCs, which were discarded. The final astrocyte monolayer was then detached from the flask using 2.5% trypsin/EDTA and seeded on poly-D-lysine (PDL)-coated glass 96 well plates for immunocytochemistry. Cells were allowed to grow for 3–4 days prior to downstream experiments to reach a 60%–70% confluence. Using this protocol, a purity of >90% was attained for both primary astrocyte and microglia cultures. Full growth media only, media containing lipopolysaccharide (LPS; 500 ng/mL; L2630-10MG, Sigma-Aldrich) or LPS + each of the neuropeptides (PACAP, VIP or Maxadilan, 100 nM) was added to the wells for 12 or 24 h prior to fixation.

2.10 | Immunocytochemistry

Untreated or treated astrocytes or microglial cells were fixed in 4% PFA (in PBS; 158127-500G, Merck) for 15 min (37°C) and washed three times with PBS. After a brief permeabilisation step (0.1% Triton X-100 in PBS, 10 min at RT), cells were blocked in a 5% BSA solution (in PBS, 3 h at RT). Primary antibody dilutions were prepared in 5% BSA (in PBS, A2153-10G, Sigma Aldrich) and incubated overnight (4°C). After a washing step, cells were incubated with secondary antibodies for 2 h at RT in the 5% BSA solution, followed by a nuclear staining step using DAPI (1:500, in PBS, 1 h at RT, D1306, Sigma-Aldrich). Following thorough washing, stained cells were kept in 100 µL PBS until imaging. Antibodies used in these experiments were: mouse-anti-GFAP (1:200, (Thermo Fisher Scientific Cat# 14-9892-82, RRID:AB_10598206)), mouse-anti-IBA1 (1:250, GeneTex Cat# GTX632426, RRID:AB_2888314), Goat-anti-Mouse FITC (1:250, Abcam Cat# ab6785, RRID:AB_955241). All images were acquired on the Leica Stellaris 8 confocal fluorescence microscope (Leica Microsystems) equipped with a 40× oil-immersion objective (NA = 1.1, Z-stack = 0.4 µm optical slices). Images were analysed in ImageJ/FIJI (version 1.53k) using maximum intensity projection images.

2.11 | Data analyses

All statistical analyses and graphs were generated using GraphPad Prism (version 9.3.1). Data are reported as the mean ± SD. To estimate normality of data, Q-Q plots of datasets were generated using GraphPad Prism software. Visual analysis demonstrating lack of skewness of data and a close alignment with the predicted 45° straight line (predictive of normal distribution) was deemed sufficient to claim that data was normally distributed. Once normal distribution was confirmed, mixed-effects ANOVA followed by Tukey's multiple comparisons tests was used to analyse both Open Field and Horizontal Ladder results. For RT-qPCR analyses, immunohistochemistry and immunofluorescence, we utilised one-way ANOVA followed by Tukey or Sidak's multiple comparisons tests, as appropriate. For the immunocytochemistry experiments, we used two-way ANOVA followed by Sidak's multiple comparisons test. p-values ≤0.05 were considered statistically significant.

3 | RESULTS

3.1 | PACAP, VIP and Maxadilan prevent locomotor deficits in cuprizone-fed mice

In this set of experiments, mice on a normal dietary regime or on a 0.2% CPZ-diet received injections of saline, PACAP, VIP or the specific PAC1 agonist Maxadilan on alternate days over the course of 4 weeks (Figure 1a,b) (Lerner et al., 2007). Maxadilan was used in view of its selective agonist activity towards the PAC1 receptor, since both PACAP and VIP exhibit strong binding affinity to PAC1, VPAC1 and VPAC2 receptors.

Upon monitoring the weight of these mice, a global weight reduction was recorded in mice intoxicated with CPZ (****$p < 0.0001$ vs. Control; Figure 1c). A similar weight loss was also seen in intoxicated mice treated with PACAP (****$p < 0.0001$ vs. Control), VIP (***$p = 0.0008$ vs. Control) and Maxadilan (****$p < 0.0001$ vs. Control). As shown, the average daily weight of all mice fed a CPZ diet was decreased, irrespective of the peptide administered, throughout the 4 weeks of treatment (Figure 1d).

Using the horizontal ladder test—also called ladder rung walking test—we assessed the effects of the neuropeptides on motor coordination and stepping accuracy in animals subjected to a CPZ diet with or without receiving neuropeptides treatment. A significant reduction of foot fault scores (indicative of deteriorated coordination) was observed in the forelimbs of mice intoxicated with 0.2% CPZ diet after 2 weeks (Figure 1e) (***$p = 0.0002$ vs. Control at Day 14), which partly worsened during the remaining 2 weeks of testing (*$p < 0.05$ and ****$p < 0.0001$ vs. Control at Day 21 and 28, respectively). Treatment with Maxadilan prevented the loss of forelimbs coordination caused by the CPZ diet from day 7 onwards, whereas signs of ameliorated coordination were observed after 2 weeks in the PACAP-treated groups. VIP treatment was able to prevent loss of forelimb coordination only after 4 weeks of treatment (#$p < 0.05$ vs. CPZ at Day 28).

Analyses of hindlimbs demonstrated similar locomotor deterioration in CPZ-fed mice (Figure 1f), with statistically significant reductions of foot fault scores in comparison with controls (****$p < 0.0001$, **$p = 0.0027$, ***$p = 0.0002$ and ****$p < 0.0001$ vs. Control at Day 7, 14, 21 and 28, respectively). As for the forelimbs, PACAP, VIP and Maxadilan treatments all ameliorated hindlimbs coordination, with a functional recovery comparable to controls starting as early as 1 week after the commencement of treatments.

In Figure 1g,h, the average error rate is shown for both the forelimbs and hindlimbs. The error rate is defined as the percentage of

errors made per step. A significant increase in the error rate was seen in mice exposed to CPZ, starting from day 14 onwards for the forelimbs (**$p=0.0063$, $p=0.0607$ and ***$p=0.0002$ vs. Control at Day 14, 21 and 28, respectively) and from day 7 onwards from the hindlimbs (****$p<0.0001$, **$p=0.0051$, ***$p=0.0002$, ***$p=0.0002$ vs. Control at Day 14, 21 and 28).

Treatment with PACAP or Maxadilan rescued the behavioural deficits caused by CPZ as early as 14 days into the diet for the forelimbs. For the hindlimbs, treatment with PACAP, VIP or Maxadilan all ameliorated CPZ-induced deficits from 7 days onwards.

The open field test is an excellent and well-established tool utilised to study mice exploratory and locomotion behaviour in mice undergoing CPZ intoxication (Kraeuter et al., 2019; Tatem et al., 2014; Wang et al., 2013; Ye et al., 2013). In the open field test, CPZ-fed mice showed a reduction in the total distance travelled starting after 2 weeks on the diet (Figure 1i,j; *$p<0.05$ vs. Control at Day 14 and 21 and **$p=0.0093$ vs. Control at Day 28). Treatment with either PACAP or Maxadilan prevented the decrease in total distance travelled caused by the CPZ diet, whereas treatment with VIP was only partly effective. In terms of exploratory behaviour (measured as the distance covered by each mouse in the centre quadrant), although slightly improved by PACAP treatment at day 21 (Figure 1k; #$p<0.05$ vs. CPZ), none of the neuropeptides mitigated the reduced exploration in mice subjected to CPZ diet. Overall, neither neuropeptide effectively improved the CPZ-induced reduction of exploration in the centre of the open field apparatus (Figure 1k).

3.2 | PACAP, VIP and Maxadilan treatment fails to prevent overall downregulation of neuropeptides and receptors genes but rescues VPAC2 expression in the white matter of cuprizone-intoxicated mice

In view of the behavioural improvements afforded by PACAP and Maxadilan in CPZ-fed mice, we sought to determine if the demyelinating diet disrupted the expression PACAP, VIP and related receptors in the white matter. Additionally, we evaluated if exogenous administration of either neuropeptide prevented any gene expression changes caused by CPZ. RT-qPCR experiments revealed that the levels of PACAP and VIP genes were significantly diminished in the corpus callosum of CPZ mice (****$p<0.0001$ vs. Control for both PACAP and VIP genes; Figure 2a,b). Exogenous administration of PACAP, VIP or Maxadilan did not prevent the downregulation in mRNA expression caused by CPZ (Figure 2a,b). PAC1 gene expression was reduced by the CPZ diet (**$p=0.0022$, Control vs. CPZ; Figure 2c) and did not return to control levels after treatment with any of the neuropeptides tested (*$p<0.05$, Control [with both PACAP and VIP]; **$p=0.0025$ [Maxadilan]). CPZ also significantly lowered VPAC1 receptor mRNA levels compared with a normal diet (****$p<0.0001$ vs. Control), and similarly to PAC1, none of the peptides were able to rescue the effects of CPZ on gene expression (Figure 2d). In contrast to PAC1 and VPAC1 transcripts, VPAC2 expression was increased by the CPZ diet (****$p<0.0001$ vs. Control; Figure 2e). This effect was ameliorated by PACAP, VIP and Maxadilan treatment (####$p<0.0001$ vs. CPZ [both PACAP and VIP], #$p<0.05$ vs. CPZ [Maxadilan]).

3.3 | The PAC1-preferring ligands PACAP and Maxadilan prevent myelin cell loss in CPZ mice

Once we established that treatment with the neuropeptides PACAP, VIP and Maxadilan prevented the locomotor deficits caused by the CPZ diet, we aimed to determine if these changes were linked to alterations in the mRNA expression of core myelin genes in the white matter. RT-qPCR analyses revealed that CPZ induced a robust reduction in the expression levels of the myelin markers *PLP1* (****$p<0.0001$ vs. Control; Figure 3a), myelin basic protein (*MBP*) (****$p<0.0001$ vs. Control; Figure 3b), myelin oligodendrocyte glycoprotein (*MOG*) (****$p<0.0001$ vs. Control; Figure 3c), and oligodendrocyte transcription factor 2 (*Olig2*) (****$p<0.0001$ vs. Control; Figure 3d). Treatment with Maxadilan, but not PACAP or VIP, partially prevented the reduction of *PLP1* (#$p<0.05$ vs. CPZ), *MOG* (#$p<0.05$) and *Olig2* (#$p<0.05$), but not *MBP* (Figure 3a–d).

PLP is the most abundant protein of CNS myelin, which plays a critical role in myelin stability and maintenance of compact lamellar structure (Knapp, 1996). Immunohistochemical analyses were performed in coronal sections of the corpus callosum spanning the rostro-caudal axis of the striatum (Figure 3a) highlighted substantial differences of PLP immunoreactivity in mice that received CPZ alone in comparison with animals that had also been injected with the peptides (Figure 3e–j). Semi-quantification of the average PLP immunoreactivity obtained from the analyses of regions of interest (ROIs) randomly selected along the medio-lateral axis of the white matter demonstrated a remarkable reduction of signal intensity in CPZ-fed mice (****$p<0.0001$ vs. Control; Figure 3k). Amongst the neuropeptide-treated groups, PLP intensity was partly preserved in CPZ mice injected with PACAP (#$p<0.05$ vs. CPZ) and, concordant with mRNA data, these effects were more pronounced in Maxadilan-injected mice (###$p<0.001$ vs. CPZ; Figure 3k). Further to these findings, we also performed Luxol Fast Blue staining in the same brain region, which demonstrated a robust reduction in the density of intact/myelinated fibres in CPZ-fed mice (****$p<0.0001$ vs. Control; Figure S1a–f). Treatment with PACAP or Maxadilan partially prevented CPZ-induced demyelination in the corpus callosum (#$p<0.05$ vs. CPZ; Figure S1A–F), whereas VIP showed no appreciable effects.

Oligodendrocyte transcription factor 2 (OLIG2) is a protein that plays a critical role in the development and differentiation of oligodendrocytes and it commonly used as a marker to identify cells committed to the oligodendrocyte lineage during development (Wegener et al., 2015; Zhou et al., 2000). Stereological analyses demonstrated that $Olig2^+$ cells were decreased in the corpus callosum of CPZ-fed mice (****$p<0.0001$ vs. Control; Figure 3l,m). Higher magnification images also showed increased cellularity in CPZ fed mice (Figure 3l, white arrowheads in lower panels). PACAP and Maxadilan, but not

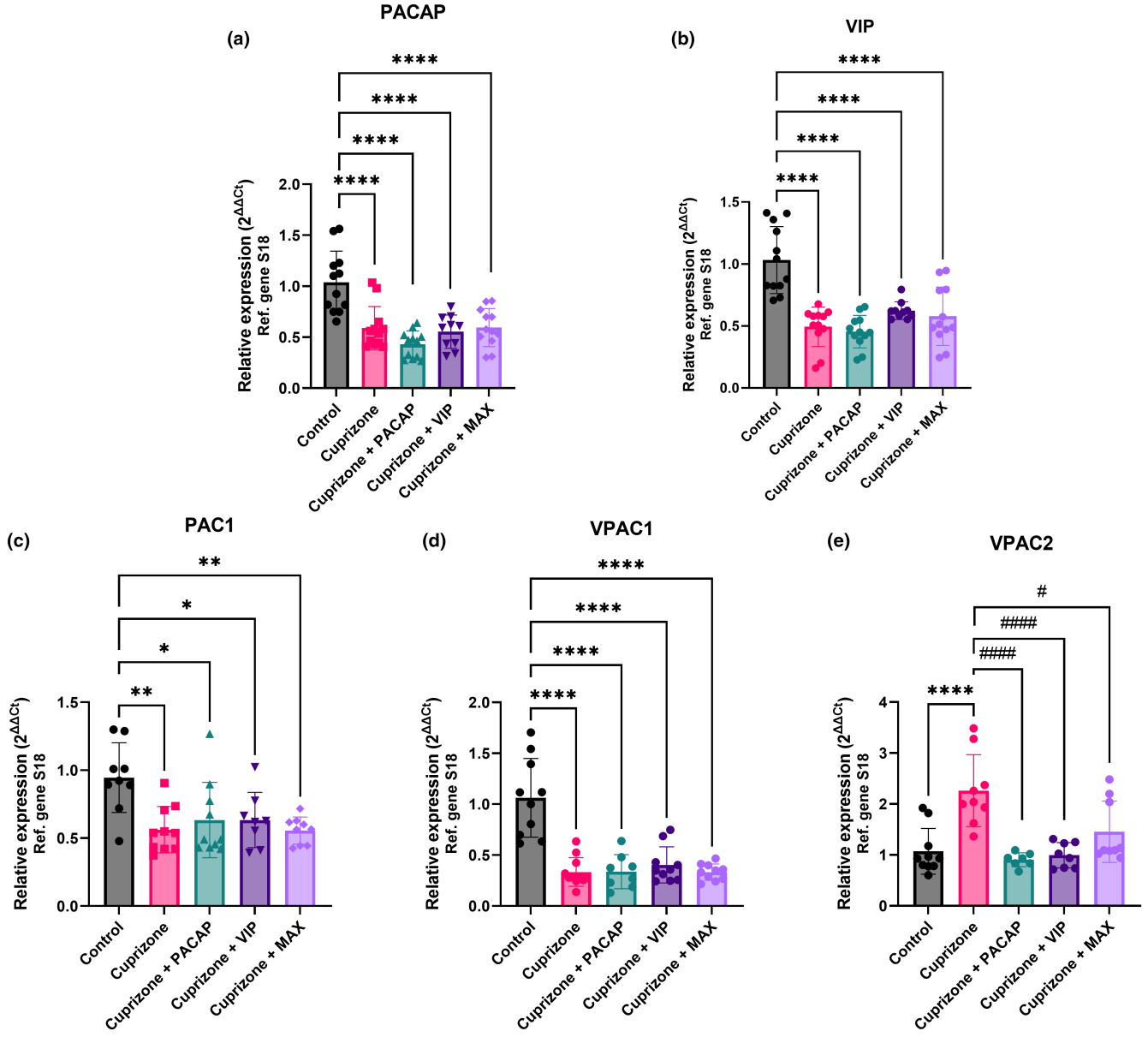

FIGURE 2 Expression levels of pituitary adenylate cyclase-activating polypeptide (PACAP), vasoactive intestinal peptide (VIP) and related receptors in the CNS white matter of mice fed a CPZ diet for 4 weeks. Real-time quantitative PCR showing the differential expression levels of (a) Adcyap1 or PACAP, (b) Vip or VIP, (c) Adcyap1r1 or PAC1, (d) Vipr1 or VPAC1 and (e) Vipr2 or VPAC2. $n = 7$–12 mice per group. Fold changes were calculated using the ΔΔCt method relative to ribosomal protein S18, the reference gene. Data shown are the mean ± SD ($n = 7$–12 mice). Statistics was computed using one-way ANOVA followed by Sidak's multiple comparisons test. $^{*}p < 0.05$, $^{**}p < 0.01$, $^{****}p < 0.0001$ vs. Control. $\#p < 0.05$ or $\#\#\#\#p < 0.0001$ vs. Cuprizone. PAC1, pituitary adenylate cyclase-activating peptide receptor 1; PACAP, pituitary adenylate cyclase-activating peptide; VIP, vasoactive intestinal peptide; VPAC1, vasoactive intestinal polypeptide receptor 1; VPAC2, vasoactive intestinal polypeptide receptor 2.

VIP, significantly increased the number of Olig2^{+} cells in the corpus callosum ($\#p < 0.05$ [PACAP] & $\#\#p = 0.0071$ [Maxadilan] vs. Cuprizone). Moreover, cellularity was decreased in animals receiving PACAP and, to a lesser extent, in those receiving Maxadilan.

As cell swelling/blistering of both the cytoplasm and nuclear compartment is a common phenomenon in damaged oligodendrocytes and/or OPCs (Dewar et al., 2003; Prineas & Parratt, 2012), we also sought to measure the mean surface size of Olig2^{+} nuclei to provide an additional indication on the extent of damage to the oligodendroglia cell lineage. We found that Olig2^{+} nuclei were increased in size both in CPZ-fed mice ($^{*}p < 0.05$ vs. Control; Figure 3n) and CPZ-fed mice receiving VIP treatment ($^{**}p = 0.0014$ vs. Control) but not in mice receiving PACAP or Maxadilan injections.

Comparative analyses of the expression of Quaking 7, the binding target of the anti-adenomatous polyposis coli (APC) antibody, were performed in the corpus callosum of demyelinated mice at a level spanning the same antero-posterior bregma interval as in Figure 3e

Journal of Neurochemistry JNC WILEY

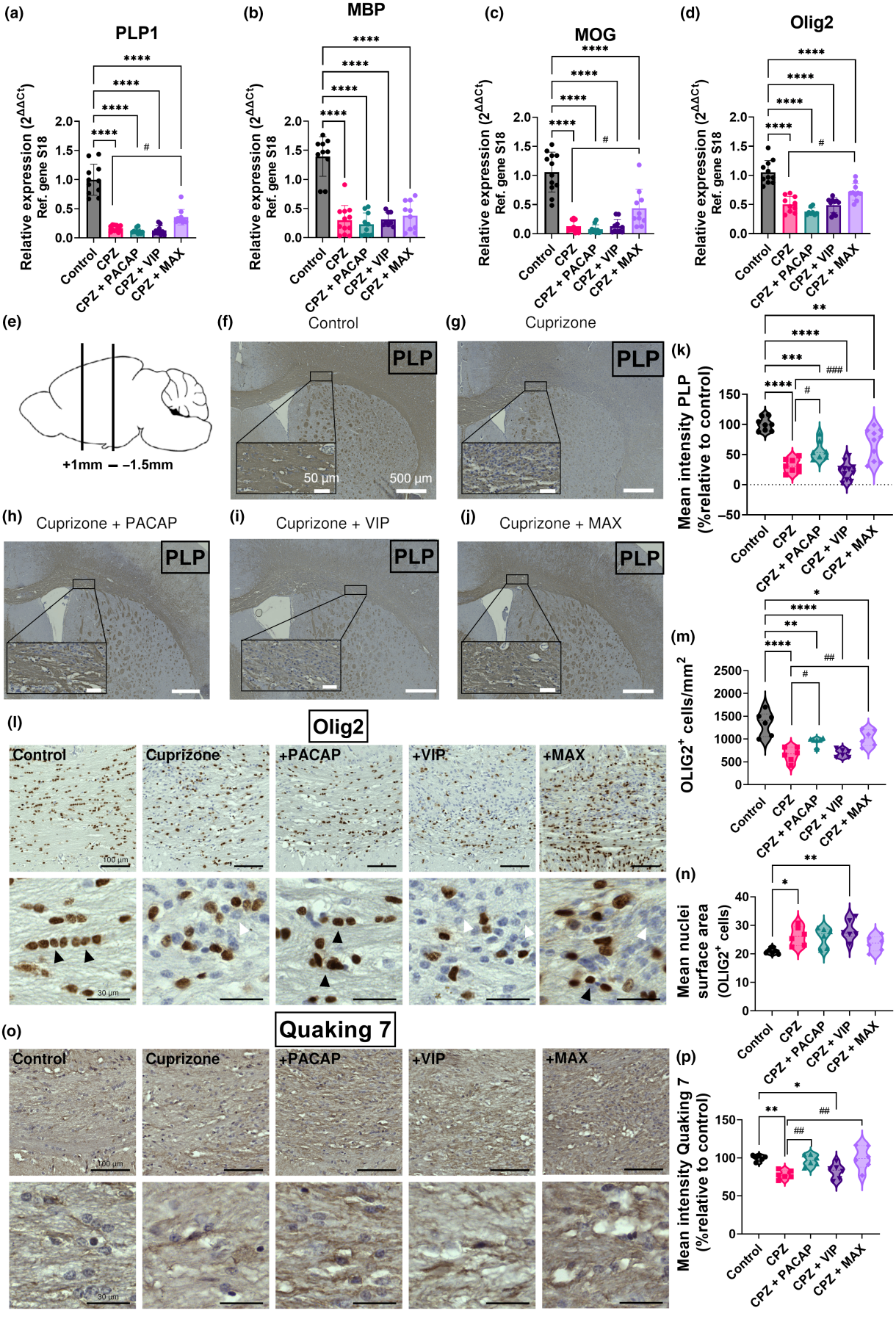

FIGURE 3 Effects of pituitary adenylate cyclase-activating polypeptide (PACAP), vasoactive intestinal peptide (VIP) and Maxadilan on myelin health after a demyelinating insult. RT-qPCR analyses demonstrating decreased gene expression of the myelin markers (a) PLP1, (b) MOG, (c) MBP, (d) Olig2 in mice fed a 0.2% cuprizone diet for a period of 4 weeks. As shown in (a), (c) and (d), Maxadilan only partly prevented CPZ-driven downregulation of myelin genes. $n = 7$–12 mice per group. Fold changes were calculated using the ΔΔCt method, using the ribosomal protein S18 as reference gene. RT-qPCR data are shown as mean ± SD. For histology, (e) shows the approximate rostro-caudal coordinates (relative to Bregma) used for the sampling of coronal brain tissue sections. Representative images depicting PLP immunoreactivity in the corpus callosum of (f) Control, (g) Cuprizone, (h) Cuprizone + PACAP, (i) Cuprizone + VIP and (j) Cuprizone + Maxadilan mice. Scale bar in (f), (g), (h), (i) and (j) = 500 μm. Scale bar in insets = 50 μm. (k) Violin plot showing the mean intensity of PLP staining measured, expressed as the percentage of control. (l) Representative low- (upper panels) and high- magnification images (lower panels) showing Olig2+ cells in the corpus callosum. Black arrowheads indicate one or more sites with at least three or more regularly aligned Olig2+ cells, whereas white arrowheads point to areas with increased cellularity due to glial cell infiltration. Stereological measurements of Olig2+ cells in the corpus callosum showing the (m) average Olig2+ cell count and (n) cell surface area. $n = 6$ mice per group. (o) Representative callosal tissue sections depicting Quaking 7 staining in the corpus callosum and (p) and semi-quantification of the mean intensity levels (relative to control). Scale bars in (l) and (o) = 100 μm (upper panels) and 30 μm (lower panels). Data were analysed using a one-way ANOVA followed by Sidak's multiple comparisons tests. $^{*}p < 0.05$, $^{**}p < 0.01$ and $^{****}p < 0.0001$ vs. Control; $\#p < 0.05$, $\#\#p < 0.01$, $\#\#\#p < 0.001$ vs. Cuprizone. MBP, myelin basic protein; MOG, myelin oligodendrocyte protein; Olig2, oligodendrocyte transcription factor 2; PLP, proteolipid protein; Quaking 7, adenomatous polyposis coli.

(Bin et al., 2016). Quaking 7 is a reliable marker for the detection of mature (myelinating) oligodendrocytes (Bin et al., 2016). Quaking 7 immunoreactivity was significantly reduced in CPZ-fed mice and CPZ-fed mice receiving VIP treatment ($^{**}p = 0.0022$ & $^{*}p < 0.05$ vs. Control; Figure 3o,p). In CPZ-fed mice treated with either PACAP or Maxadilan, both successfully prevented the attenuation of Quaking 7 staining, which reached levels to comparable to control mice ($\#\#p = 0.0097$ [PACAP] & $\#\#p = 0.0022$ [Maxadilan] vs. Cuprizone).

3.4 | PACAP, VIP and Maxadilan attenuate cuprizone-induced axonopathy, neuronal and synaptic loss

The major contributing factor to clinical disability in MS is the progressive axonal damage and neuronal loss in afflicted people (Fisher et al., 2008; Trapp & Nave, 2008). This pathological feature has also been observed in EAE mice and in the CPZ demyelination model (Slowik et al., 2015; Wagenknecht et al., 2016).

Here we assessed if PACAP, VIP or Maxadilan treatment prevented axonopathy, neuronal damage and synaptic loss in mice subjected to the CPZ diet (Figure 4). In both the corpus callosum and striatum, the CPZ diet caused a robust reduction in the staining intensity of the class III beta-tubulin (aka TUJ1)—a pan-neuronal/axonal marker (Caccamo et al., 1989)—in comparison with control mice ($^{****}p < 0.0001$ vs. Control [Corpus callosum], $^{****}p < 0.0001$ vs. Control [Striatum]; Figure 4a,b,d,e). Interestingly, all three neuropeptides equally prevented the reduction of TUJ1 staining caused by the demyelinating diet both in the corpus callosum ($\#\#p = 0.002$ [PACAP], $\#\#p = 0.004$ [VIP] and $\#\#p = 0.0025$ [Maxadilan] vs. CPZ; Figure 5a,b) and striatum ($\#\#\#p = 0.001$ [PACAP], $\#\#\#p = 0.0009$ [VIP], $\#\#\#\#p < 0.0001$ [Maxadilan] vs. CPZ; Figure 4d,e). To complement our findings with TUJ1, we also assessed levels of Neurofilament protein light chain (NF-L). NF-L is commonly used to indicate axonal damage (Cebulla et al., 2023; Martin-Aguilar et al., 2020; van den Bosch et al., 2022). NF-L staining intensity increased in CPZ-fed mice ($^{****}p < 0.0001$ vs. Control; Figure 4c), with neuropeptide treatment reducing NF-L levels back to control levels ($\#\#\#p = 0.001$ [PACAP], $\#\#p = 0.0014$ [VIP], $\#\#\#\#p < 0.0001$ [Maxadilan] vs. CPZ; Figure 4c).

To assess if CPZ intoxication would lead to striatal synaptic loss, striatal sections were co-stained with synaptophysin, a marker used to identify synaptic terminals (Scheuer et al., 2022). Semi-quantification of synaptophysin immunoreactivity showed a clear loss of synaptic density in the striatum of CPZ-fed mice ($^{****}p < 0.0001$ vs. Control; Figure 4c,d), an effect that was prevented by either PACAP or Maxadilan ($\#\#\#\#p < 0.0001$ [PACAP], $\#\#\#\#p < 0.0001$ [Maxadilan] vs. CPZ), but not VIP.

3.5 | Treatment with PACAP or Maxadilan decreases the expression of the inflammatory markers GFAP and IBA1 in the corpus callosum of cuprizone-intoxicated mice

Glial fibrillary acidic protein (*GFAP*) gene encodes for a protein that is highly abundant in astrocytes and whose expression is induced upon an inflammatory challenge (Yang & Wang, 2015). Our analyses revealed that the CPZ diet caused a robust increase in *GFAP* gene expression ($^{****}p < 0.0001$ vs. Control; Figure 5a), suggestive of astrogliosis. Treatment with either PACAP, VIP or Maxadilan prevented *GFAP* gene induction caused by the CPZ diet ($\#\#\#\#p < 0.0001$ vs. CPZ [PACAP]; $\#p < 0.05$ [VIP]; $\#\#\#\#p < 0.0001$ [Maxadilan]).

Similarly to GFAP, ionised calcium-binding adapter molecule 1 (*IBA1*) is a well-established marker of microglial cells, indicating both pro-inflammatory and anti-inflammatory phenotypes (Walker & Lue, 2015), although in this instance it likely reflected pro-inflammatory activation. As expected, upon receiving the CPZ diet, *IBA1* transcripts were significantly increased ($^{****}p < 0.0001$ vs. Control; Figure 5b). Treatment with PACAP and Maxadilan, but not VIP, significantly reduced *IBA1* mRNA levels ($\#p < 0.05$ vs. CPZ [PACAP]; $\#\#\#\#p < 0.0001$ [Maxadilan] vs. Cuprizone).

To corroborate our mRNA findings, predominantly suggesting that the beneficial effects of PACAP and Maxadilan in astrocytes

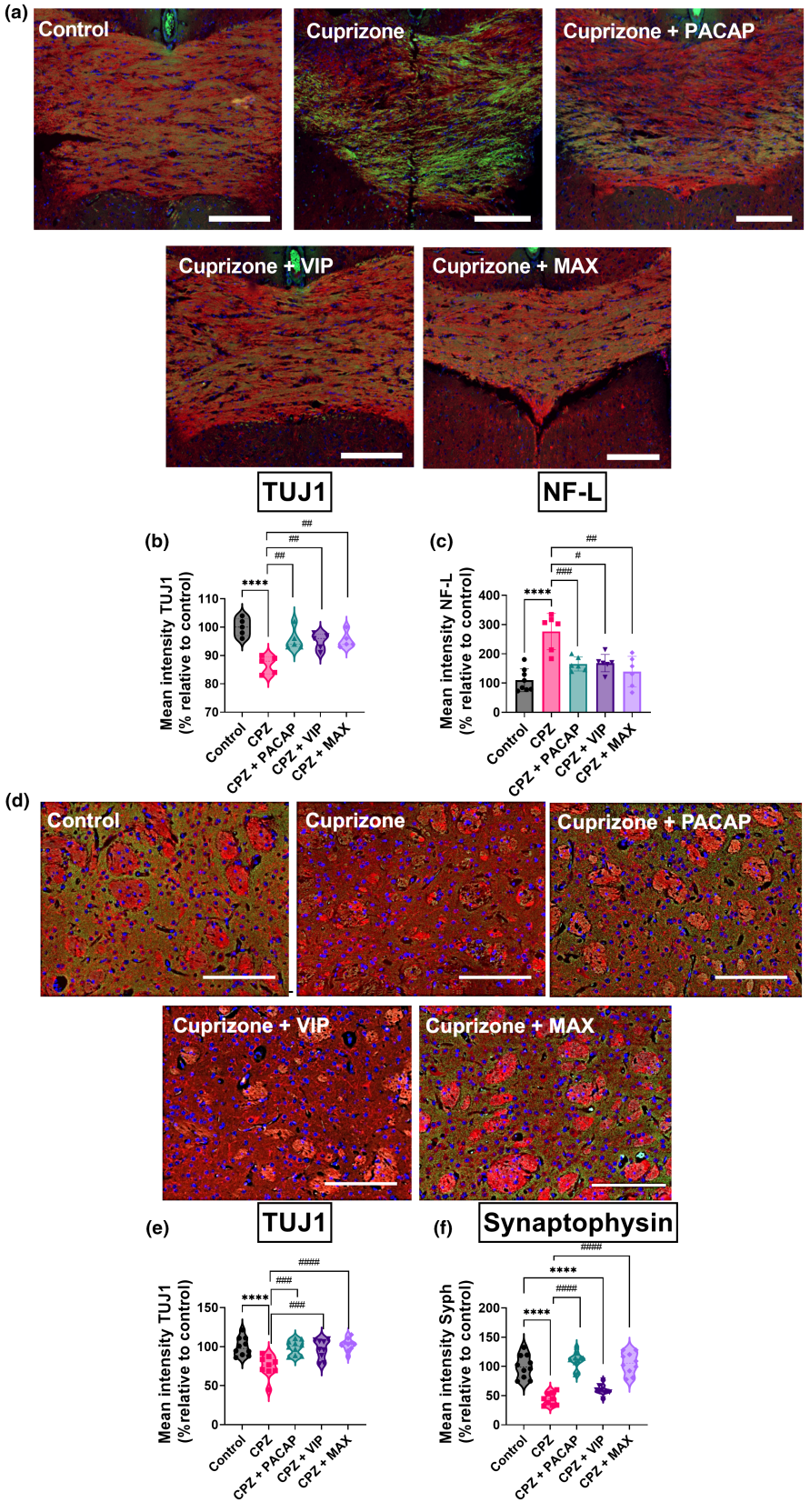

FIGURE 4 Protective effects of the neuropeptides against cuprizone-induced axonopathy, neuronal and synaptic loss. (a) Representative images of TUJ1 (red) and NF-L (green) co-staining in the corpus callosum of CPZ-fed mice after 4 weeks. Nuclei were counterstained with DAPI (blue). Scale bar = 200 μm. $n = 5–9$ mice per group. Violin plot showing the (b) average TUJ1 staining intensity and (c) NF-L staining intensity of axons in the corpus callosum of each treatment group are presented. (d) Representative images of striatal sections (antero-posterior +1 mm to −1.5 mm from Bregma) co-stained with Synaptophysin (green) and TUJ1 (red). Scale bar = 100 μm. $n = 9–10$ mice. Quantification of (e) synaptophysin and (f) TUJ1 staining intensities in the corpus striatum. Data shown are the mean fluorescence intensities (relative to control), expressed as percentages. $^{****}p < 0.0001$ vs. Control. $\#p < 0.05$, $\#\#p < 0.01$, $\#\#\#p < 0.001$ or $\#\#\#\#p < 0.0001$ vs. Cuprizone, as determined by one-way ANOVA and Tukey post-hoc test. NF-L, Neurofilament light chain; Syph, synaptophysin; TUJ1, class III beta-tubulin.

and microglia were PAC1-mediated, we conducted additional immunofluorescence experiments in the corpus callosum of mice subjected to the same experimental conditions (Figure 5c–e). In line with RNA data, CPZ-fed animals showed robust astrocytic activation, as indicated by the significant increase in GFAP$^+$ cells in the corpus callosum ($^{****}p < 0.0001$ vs. Control; Figure 5c,d). PACAP treatment partly prevented CPZ-driven GFAP up-regulation ($\#\#\#\#p < 0.001$ vs. CPZ). These beneficial effects were also seen in Maxadilan-treated

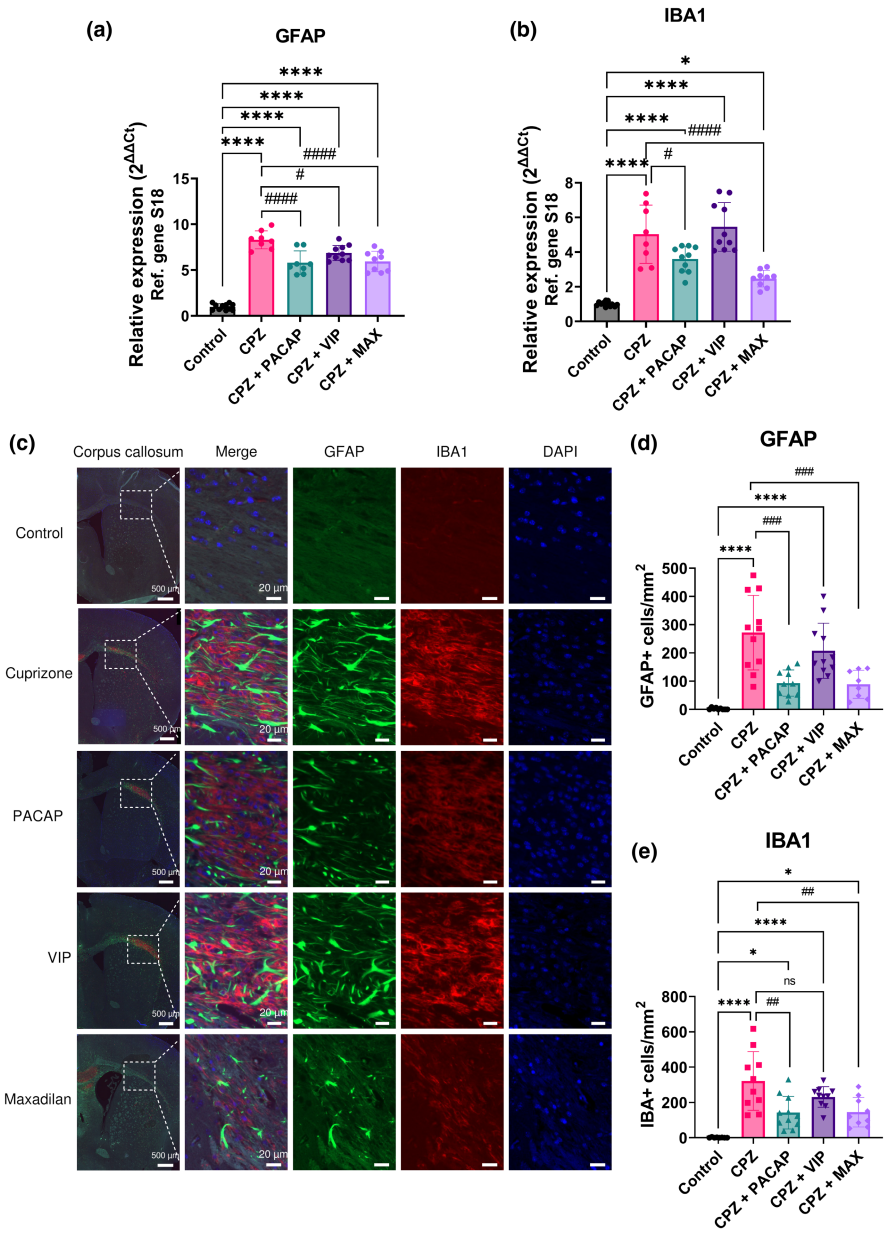

FIGURE 5 Pituitary adenylate cyclase-activating polypeptide (PACAP) and Maxadilan attenuate astrogliosis and microgliosis in the corpus callosum of CPZ-fed mice after 4 weeks. Relative mRNA expression of (a) GFAP and (b) IBA1 was determined using RT-qPCR. Fold changes were calculated using the ΔΔCt method, using ribosomal protein S18 as the housekeeping gene. Results are presented as mean fold change values ± SD, using 10–12 mice per group. (c) Representative photomicrographs of the corpus callosum (antero-posterior +1 mm to −1.5 mm from Bregma) co-stained with GFAP and IBA1 from mice fed a standard diet (Control) or a 0.2% CPZ diet and injected with either saline, PACAP, VIP or Maxadilan. Number of (d) GFAP$^+$ and (e) IBA1$^+$ cells per mm^2 are depicted in bar graphs ($n = 10–12$ mice). One-way ANOVA followed by Sidak's multiple comparison's test was used to assess statistical significance. $^*p < 0.05$, $^{****}p < 0.0001$ vs. control; $\#p < 0.05$, $\#\#p < 0.01$, $\#\#\#p < 0.001$, $\#\#\#\#p < 0.0001$ vs. CPZ. GFAP, glial fibrillary acidic protein; IBA1, ionised calcium-binding adapter molecule 1.

mice ($\#\#\#p = 0.0002$ vs. CPZ). In contrast, VIP treatment failed to prevent astrocytic activation, as the number of GFAP$^+$ cells in the corpus callosum did not differ from CPZ mice.

IBA1$^+$ cell count was also robustly increased in the corpus callosum of CPZ-fed mice ($^{****}p < 0.0001$ vs. Control; Figure 5c,e). PACAP and Maxadilan significantly reduced the number of IBA1+ cells in the corpus callosum ($\#\#p = 0.001$ vs. CPZ [PACAP]; $\#\#p = 0.0024$ [Maxadilan]; Figure 5e), whereas VIP did not (Figure 5c,e).

3.6 | PAC1 receptor-mediated anti-inflammatory effects stem predominantly from astrocytes

Given that CPZ has no direct effects on astrocytes or microglia, our next step was to dissect the individual contributions of these glial cell populations to the anti-inflammatory responses triggered by the neuropeptides. For this purpose, primary astrocyte and microglial cultures were challenged with the inflammatory mimetic lipopolysaccharide (LPS) and co-treated with each neuropeptide for either 12 or 24 h. Representative photomicrographs and related quantifications are depicted in Figure 6.

In line with our in vivo findings, PACAP and Maxadilan, but not VIP, reduced LPS-induced astrocytosis in primary cultures after 12 h ($\#\#\#\#p < 0.0001$ for both PACAP and Maxadilan vs. LPS at 12 h; Figure 6a,b). After 24 h LPS exposure, all three neuropeptides were able to dampen astrocyte activation ($\#\#\#\#p < 0.0001$ [PACAP], $\#\#p = 0.0048$ [VIP], $\#\#\#\#p < 0.0001$ [Maxadilan] vs. LPS at 24 h).

In primary microglia, LPS-induced microgliosis was prevented solely by PACAP treatment at the 12 h time point ($\#\#\#\#p < 0.0001$ vs. LPS at 12 h; Figure 6d,e). After 24 h, both PACAP and VIP, but not Maxadilan, diminished IBA1 intensity ($\#\#\#\#p < 0.0001$ [PACAP], $\#\#\#\#p < 0.0001$ [VIP] vs. LPS at 24 h).

These results imply that the anti-inflammatory effects of the neuropeptides in isolated microglial cultures may also involve the co-activation of VPAC1 and VPAC2 receptors, in addition to PAC1 receptors.

4 | DISCUSSION

In this study, we explored the potential therapeutic benefits of treatment with either PACAP, VIP or the PAC1-specific agonist Maxadilan in the cuprizone mouse model of demyelination. Our experiments demonstrated consistent improvements in locomotor performance and motor coordination in animals treated with either PACAP or Maxadilan, and less so in animals treated with VIP. These findings were corroborated by histopathological/immunohistochemical evidence indicating robust protective activities of the two PAC1-preferring ligands against cuprizone-induced myelin loss. We also observed reversal of astro- and microgliosis in the demyelinating corpus callosum after treatment with these neuropeptides. However, further in vitro studies revealed that PAC1-driven ameliorative effects were mostly seen in astrocytes, rather than in microglia, suggesting a novel and perhaps overlooked cell-specific responsiveness to this class of neuropeptides.

Since PACAP and Maxadilan elicited equipotent ameliorative effects, our results emphasise the role of the PAC1 receptor in mediating a protective response within the CNS white matter of mice undergoing experimentally induced demyelination. To our knowledge, these findings pinpoint for the first time the importance of targeting PAC1 receptors as a possible therapeutic strategy to prevent myelin loss and reduce CNS white matter inflammation following a primary acute demyelinating event.

Currently, several animal models of MS have been developed in the attempt to uncover disease complexity and identify possible cures, each with their own benefits and limitations (Lassmann & Bradl, 2017; Ransohoff, 2012). The cuprizone model is recognised as a suitable preclinical model of demyelination, as animals on a four

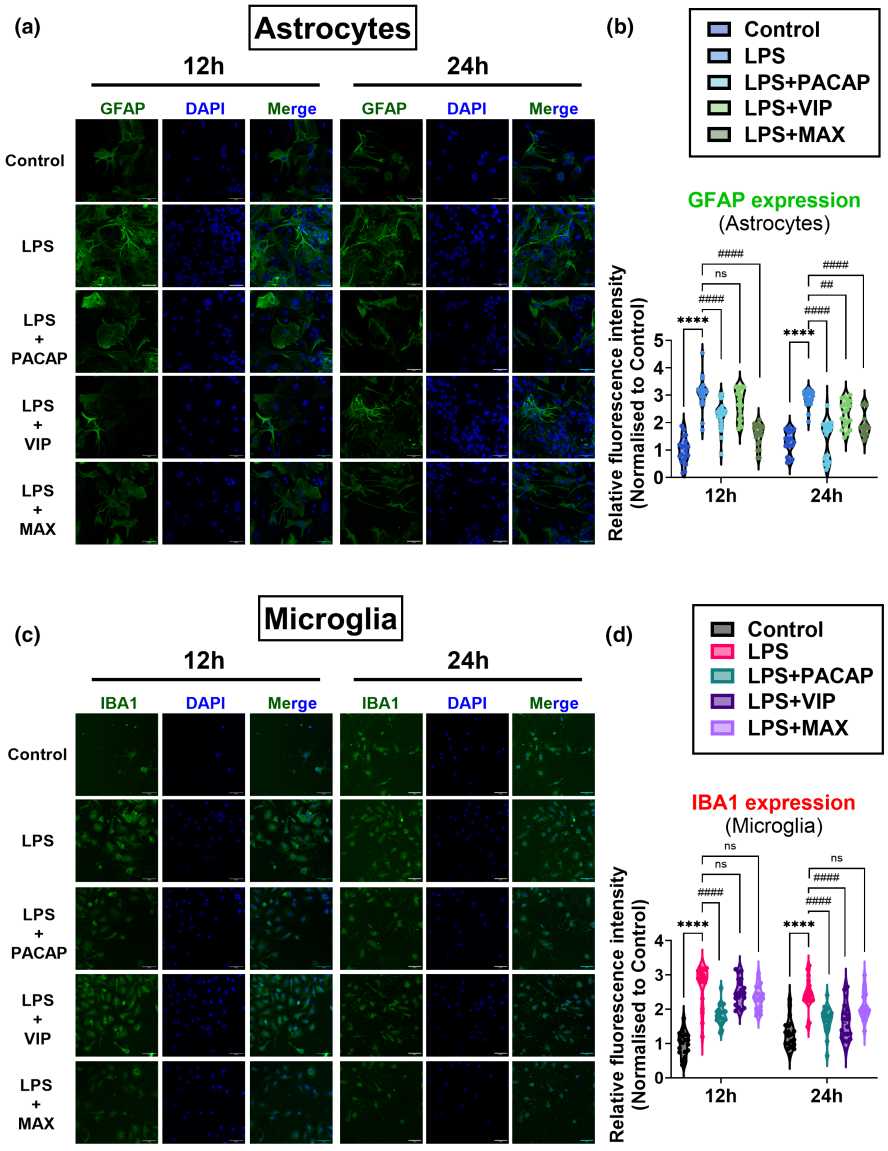

FIGURE 6 Anti-inflammatory effects of Pituitary adenylate cyclase-activating polypeptide (PACAP), vasoactive intestinal peptide (VIP) and Maxadilan in primary glia cells challenged with lipopolysaccharide (LPS). (a) Representative photomicrographs of primary murine astrocytes treated with LPS (500 ng/mL) alone, LPS + PACAP, +VIP or +Maxadilan (all used at 100 nM concentration) after 12 or 24 h and stained for GFAP (green) and DAPI (blue). Untreated cells were used as controls. Scale bar = 50 μm. (b) Quantification of GFAP fluorescence ($n = 9$–15 ROIs/three independent experiments). (c) Representative photomicrographs of primary murine microglia exposed to the same treatments/conditions as in (a), but stained for IBA1 (green) and nuclei counterstained with DAPI (blue). (d) Quantification of IBA1 fluorescence ($n = 7$–14 ROIs/three independent experiments). Data in (b) and (d) was analysed using two-way ANOVA followed by Sidak's multiple comparison's test. ****$p < 0.0001$ vs. control; ##$p < 0.01$, ####$p < 0.0001$ vs. LPS at the corresponding time point. GFAP, glial fibrillary acidic protein; IBA1, ionised calcium-binding adapter molecule 1.

week cuprizone dietary regime develop white matter loss consistent with type III MS lesions in humans, whilst also offering the opportunity to understand the dynamic interplay of demyelination/remyelination that is seen in clinic (Ludwin, 1978; Tsiperson et al., 2010; Yamanaka et al., 2023; Zhang et al., 2019). In this study, we focussed on the role of PACAP and VIP treatment during demyelination as we were interested in unveiling any mitigating effects of these neuropeptides during a damaging insult to CNS myelin. Future research investigating whether targeting PAC1 (or perhaps other PACAP/VIP receptors) may also play a role in promoting spontaneous myelin recovery may offer additional insights on the spectrum of beneficial activities elicited by these neuropeptides. However, this remains beyond the scope of our current study.

Another commonly used animal model of MS is the model of experimental autoimmune encephalitis (EAE). Using this model, researchers have shown that PACAP ameliorated clinical symptoms and improved disease course via its anti-inflammatory properties (Kato et al., 2004). Additionally, PACAP-deficient mice showed worsened EAE, further emphasising the immune- and possibly neuro- and myelo-protective activities of this peptide in other MS models (Tan et al., 2009, 2013). Moreover, several studies have shown the beneficial impact of PACAP in stimulating myelin regeneration in the peripheral nervous system (Armstrong et al., 2008; Castorina et al., 2008, 2014). In vitro, endogenous PACAP and exogenously applied PACAP stimulate the proliferation of oligodendrocyte progenitor cells, although it inhibits cell maturation (Lee et al., 2001; Vincze et al., 2011). The results from our study are in line with these findings, as PACAP-treated mice show some degree of myelin preservation—likely caused by its peripheral anti-inflammatory effects—in the cuprizone demyelination model. Moreover, we have reason to believe that the effects seen are mediated via the agonistic activity on the PAC1 receptor, since administration of the selective receptor agonist Maxadilan produced similar, if not more potent protective effects than PACAP in the CNS white matter.

To our surprise, whilst we also observed some locomotor improvements in CPZ mice injected with VIP, we did not detect any significant histological or molecular signs of myelin preservation. These findings partly align with previously reported effects in VIP-deficient mice subjected to EAE, where animals showed impaired parenchymal CD4 T cells infiltration and reduced CNS inflammatory burden, suggesting that VIP plays an unanticipated permissive and/or proinflammatory role in the propagation of the inflammatory response in the CNS (Abad et al., 2010). The fact that VIP treatment was still able to prevent neurological deterioration in CPZ mice is likely due to its protective activities in neurons. In this respect, we report that all the three neuropeptides tested, including VIP, were able to preserve TUJ1 and NF-L expression at levels similar to controls in axons travelling through the corpus callosum, suggesting reduced axonal damage. Furthermore, although VIP was unable to maintain synaptic density in the striatum of CPZ-fed mice, it prevented TUJ1 downregulation in neurons/axons, which could explain why clinical and locomotor performance was partly improved even in mice treated with VIP. Additionally, the VIP peptide is known to promote neuronal disinhibition, through activation of VPAC1 receptors, or enhanced pyramidal cell excitability, through activation of VPAC2 receptors (Cunha-Reis & Caulino-Rocha, 2020). Therefore, it cannot be excluded that in VIP-treated animals, some of the persisting locomotor deficits may have been hidden by the excitatory activities elicited by the peptide.

A further point worth considering is that VIP targets both VPAC receptors with similar affinity; however, studies using immunised VIP receptor knock-out mice showed opposing results (Abad et al., 2016; Fernandez-Martin et al., 2006; Tan et al., 2015). As mentioned, VPAC1-deficient mice displayed resistance to EAE induction whereas VPAC2-deficiency exacerbated EAE pathology. In addition, from a pharmacokinetic perspective, VIP blood–brain-barrier permeability seems to be lower than PACAP (Banks et al., 1993; Dogrukol-Ak et al., 2003). Although our results suggest that the main effect of the peptides is likely to be peripheral, as rapid systemic degradation interferes with CNS bioavailability (Lambeir et al., 2001), the potent central neuroprotective effects of the neuropeptides still support this theory. In fact, Maxadilan, which does not have any significant sequence homology with PACAP and therefore may evade systemic enzymatic inactivation (Moro et al., 1999), produced more robust therapeutic effects than PACAP, especially in terms of myelin protection.

Interestingly, in vitro studies in primary astrocytes and microglia revealed some cell-specific differences in the responses to these neuropeptides under inflammatory conditions. Specifically, both PACAP and Maxadilan strongly reduced astrocytic polarisation in cells challenged with LPS within 12 h, suggesting a PAC1-mediated effect. In contrast, PACAP and VIP (but not Maxadilan) reliably prevented polarisation in LPS-treated primary microglia, suggesting the involvement of VPAC-type receptors in the anti-inflammatory response of the neuropeptides.

However, further research is warranted to dissect both the cell-specific contributions to the ameliorative properties of these neuropeptides, as well as assessing the central vs. peripheral differences in the activities of both neuropeptides in the context of demyelinating pathologies, such as in MS. Moreover, additional studies using conditional/inducible mice models may help dissecting the cell-specific contributions of PAC1 receptors to myelin protection and regeneration.

In conclusion, this study provides novel evidence that targeting PAC1 receptors is sufficient to mitigate myelin loss and locomotor deficits during an acute demyelination challenge. The study highlights the potent anti-inflammatory and neuroprotective potential of this receptor subtype in the CPZ model of MS. Convergent behavioural and histopathological data emphasised a protective activity by this class of peptides, which adds important knowledge that may be utilised to instigate novel investigations aimed to exploit this therapeutic target as a novel DMT for demyelinating disorders.

AUTHOR CONTRIBUTIONS

Margo I. Jansen: Investigation; formal analysis; writing – original draft; writing – review and editing; methodology; validation;

visualization. **Yasir Mahmood:** Investigation; formal analysis; methodology. **Jordan Lee:** Investigation; formal analysis; methodology. **Sarah Thomas Broome:** Investigation; methodology. **James A. Waschek:** Writing – review and editing. **Alessandro Castorina:** Conceptualization; writing – review and editing; funding acquisition; project administration; resources; supervision; data curation; formal analysis.

ACKNOWLEDGEMENTS

We would like to acknowledge the technical support from Ms Sarah Osvath during the conduction of molecular experiments and Ms Fiona Ryan (Animal Facility Manager) for her ongoing guidance with animal work. The authors acknowledge the use of the equipment Zeiss Axioscan Z1 in the Microbial Imaging Facility in the Faculty of Science at the University of Technology Sydney. We would like to thank A/Prof. Louise Cole for her scientific input and technical assistance. This research was funded by the Rebecca L. Cooper Medical Research Foundation (Grant no. PG2020710) to A/Prof. Alessandro Castorina. Open access publishing facilitated by University of Technology Sydney, as part of the Wiley - University of Technology Sydney agreement via the Council of Australian University Librarians.

CONFLICT OF INTEREST STATEMENT

The authors declare no competing interests.

DATA AVAILABILITY STATEMENT

Raw data and images can be made available upon reasonable request to authors.

ORCID

Margo I. Jansen https://orcid.org/0000-0003-0721-4055
Sarah Thomas Broome https://orcid.org/0000-0002-5444-0920
James A. Waschek https://orcid.org/0000-0003-2727-9876
Alessandro Castorina https://orcid.org/0000-0001-7037-759X

REFERENCES

Abad, C., Jayaram, B., Becquet, L., Wang, Y., O'Dorisio, M. S., Waschek, J. A., & Tan, Y. V. (2016). VPAC1 receptor (Vipr1)-deficient mice exhibit ameliorated experimental autoimmune encephalomyelitis, with specific deficits in the effector stage. *Journal of Neuroinflammation*, *13*, 169.

Abad, C., Tan, Y. V., Lopez, R., Nobuta, H., Dong, H., Phan, P., Feng, J. M., Campagnoni, A. T., & Waschek, J. A. (2010). Vasoactive intestinal peptide loss leads to impaired CNS parenchymal T-cell infiltration and resistance to experimental autoimmune encephalomyelitis. *Proceedings of the National Academy of Sciences of the United States of America*, *107*, 19555–19560.

Abad, C., & Waschek, J. A. (2011). Immunomodulatory roles of VIP and PACAP in models of multiple sclerosis. *Current Pharmaceutical Design*, *17*, 1025–1035.

Armstrong, B. D., Abad, C., Chhith, S., Cheung-Lau, G., Hajji, O. E., Nobuta, H., & Waschek, J. A. (2008). Impaired nerve regeneration and enhanced neuroinflammatory response in mice lacking pituitary adenylyl cyclase activating peptide. *Neuroscience*, *151*, 63–73.

Banks, W. A., Kastin, A. J., Komaki, G., & Arimura, A. (1993). Passage of pituitary adenylate cyclase activating polypeptide1-27 and pituitary adenylate cyclase activating polypeptide1-38 across the blood-brain barrier. *The Journal of Pharmacology and Experimental Therapeutics*, *267*, 690–696.

Barnett, M. H., & Prineas, J. W. (2004). Relapsing and remitting multiple sclerosis: Pathology of the newly forming lesion. *Annals of Neurology*, *55*, 458–468.

Bin, J. M., Harris, S. N., & Kennedy, T. E. (2016). The oligodendrocyte-specific antibody 'CC1' binds quaking 7. *Journal of Neurochemistry*, *139*, 181–186.

Caccamo, D., Katsetos, C. D., Herman, M. M., Frankfurter, A., Collins, V. P., & Rubinstein, L. J. (1989). Immunohistochemistry of a spontaneous murine ovarian teratoma with neuroepithelial differentiation. Neuron-associated beta-tubulin as a marker for primitive neuroepithelium. *Laboratory Investigation*, *60*, 390–398.

Castorina, A., Scuderi, S., D'Amico, A. G., Drago, F., & D'Agata, V. (2014). PACAP and VIP increase the expression of myelin-related proteins in rat schwannoma cells: Involvement of PAC1/VPAC2 receptor-mediated activation of PI3K/Akt signaling pathways. *Experimental Cell Research*, *322*, 108–121.

Castorina, A., Tiralongo, A., Giunta, S., Carnazza, M. L., Rasi, G., & D'Agata, V. (2008). PACAP and VIP prevent apoptosis in schwannoma cells. *Brain Research*, *1241*, 29–35.

Cebulla, N., Schirmer, D., Runau, E., Flamm, L., Gommersbach, S., Stengel, H., Zhou, X., Einsele, H., Reinhold, A. K., Rogalla von Bieberstein, B., Zeller, D., Rittner, H., Kortüm, K. M., & Sommer, C. (2023). Neurofilament light chain levels indicate acute axonal damage under bortezomib treatment. *Journal of Neurology*, *270*, 2997–3007.

Compston, A., & Coles, A. (2008). Multiple sclerosis. *Lancet*, *372*, 1502–1517.

Cunha-Reis, D., & Caulino-Rocha, A. (2020). VIP modulation of hippocampal synaptic plasticity: A role for VIP receptors as therapeutic targets in cognitive decline and mesial temporal lobe epilepsy. *Frontiers in Cellular Neuroscience*, *14*, 153.

Cunniffe, N., & Coles, A. (2021). Promoting remyelination in multiple sclerosis. *Journal of Neurology*, *268*, 30–44.

Dargahi, N., Katsara, M., Tselios, T., Androutsou, M. E., de Courten, M., Matsoukas, J., & Apostolopoulos, V. (2017). Multiple sclerosis: Immunopathology and treatment update. *Brain Sciences*, *7*, 78.

Delgado, M., Martinez, C., Pozo, D., Calvo, J. R., Leceta, J., Ganea, D., & Gomariz, R. P. (1999). Vasoactive intestinal peptide (VIP) and pituitary adenylate cyclase-activation polypeptide (PACAP) protect mice from lethal endotoxemia through the inhibition of TNF-alpha and IL-6. *Journal of Immunology*, *162*, 1200–1205.

Dewar, D., Underhill, S. M., & Goldberg, M. P. (2003). Oligodendrocytes and ischemic brain injury. *Journal of Cerebral Blood Flow & Metabolism*, *23*, 263–274.

Dogrukol-Ak, D., Banks, W. A., Tuncel, N., & Tuncel, M. (2003). Passage of vasoactive intestinal peptide across the blood-brain barrier. *Peptides*, *24*, 437–444.

Fernandez-Martin, A., Gonzalez-Rey, E., Chorny, A., Martin, J., Pozo, D., Ganea, D., & Delgado, M. (2006). VIP prevents experimental multiple sclerosis by downregulating both inflammatory and autoimmune components of the disease. *Annals of the New York Academy of Sciences*, *1070*, 276–281.

Fisher, E., Lee, J. C., Nakamura, K., & Rudick, R. A. (2008). Gray matter atrophy in multiple sclerosis: A longitudinal study. *Annals of Neurology*, *64*, 255–265.

Franco-Pons, N., Torrente, M., Colomina, M. T., & Vilella, E. (2007). Behavioral deficits in the cuprizone-induced murine model of demyelination/remyelination. *Toxicology Letters*, *169*, 205–213.

Franklin, R. J. M., & Simons, M. (2022). CNS remyelination and inflammation: From basic mechanisms to therapeutic opportunities. *Neuron*, *110*, 3549–3565.

Gajofatto, A., & Benedetti, M. D. (2015). Treatment strategies for multiple sclerosis: When to start, when to change, when to stop? *World Journal of Clinical Cases*, *3*, 545–555.

Ghaiad, H. R., Nooh, M. M., El-Sawalhi, M. M., & Shaheen, A. A. (2017). Resveratrol promotes remyelination in cuprizone model of multiple sclerosis: Biochemical and histological study. *Molecular Neurobiology*, *54*, 3219–3229.

Hauser, S. L., & Cree, B. A. C. (2020). Treatment of multiple sclerosis: A review. *The American Journal of Medicine*, *133*, 1380–1390.e2.

Hochstrasser, T., Exner, G. L., Nyamoya, S., Schmitz, C., & Kipp, M. (2017). Cuprizone-containing pellets are less potent to induce consistent demyelination in the corpus callosum of C57BL/6 mice. *Journal of Molecular Neuroscience*, *61*, 617–624.

Jansen, M. I., Thomas Broome, S., & Castorina, A. (2022). Exploring the pro-phagocytic and anti-inflammatory functions of PACAP and VIP in microglia: Implications for multiple sclerosis. *International Journal of Molecular Sciences*, *23*, 4788.

Kajimura, J., Ito, R., Manley, N. R., & Hale, L. P. (2016). Optimization of single- and dual-color immunofluorescence protocols for formalin-fixed, paraffin-embedded archival tissues. *The Journal of Histochemistry and Cytochemistry*, *64*, 112–124.

Karunia, J., Niaz, A., Mandwie, M., Thomas Broome, S., Keay, K. A., Waschek, J. A., Al-Badri, G., & Castorina, A. (2021). PACAP and VIP modulate LPS-induced microglial activation and trigger distinct phenotypic changes in murine BV2 microglial cells. *International Journal of Molecular Sciences*, *22*, 10947.

Kato, H., Ito, A., Kawanokuchi, J., Jin, S., Mizuno, T., Ojika, K., Ueda, R., & Suzumura, A. (2004). Pituitary adenylate cyclase-activating polypeptide (PACAP) ameliorates experimental autoimmune encephalomyelitis by suppressing the functions of antigen presenting cells. *Multiple Sclerosis*, *10*, 651–659.

Knapp, P. E. (1996). Proteolipid protein: Is it more than just a structural component of myelin? *Developmental Neuroscience*, *18*, 297–308.

Kraeuter, A. K., Guest, P. C., & Sarnyai, Z. (2019). The open field test for measuring locomotor activity and anxiety-like behavior. *Methods in Molecular Biology*, *1916*, 99–103.

Lambeir, A. M., Durinx, C., Proost, P., Van Damme, J., Scharpé, S., & De Meester, I. (2001). Kinetic study of the processing by dipeptidyl-peptidase IV/CD26 of neuropeptides involved in pancreatic insulin secretion. *FEBS Letters*, *507*, 327–330.

Lassmann, H., & Bradl, M. (2017). Multiple sclerosis: Experimental models and reality. *Acta Neuropathologica*, *133*, 223–244.

Lee, M., Lelièvre, V., Zhao, P., Torres, M., Rodriguez, W., Byun, J. Y., Doshi, S., Ioffe, Y., Gupta, G., de los Monteros, A. E., de Vellis, J., & Waschek, J. (2001). Pituitary adenylyl cyclase-activating polypeptide stimulates DNA synthesis but delays maturation of oligodendrocyte progenitors. *The Journal of Neuroscience*, *21*, 3849–3859.

Lerner, E. A., Iuga, A. O., & Reddy, V. B. (2007). Maxadilan, a PAC1 receptor agonist from sand flies. *Peptides*, *28*, 1651–1654.

Liebetanz, D., & Merkler, D. (2006). Effects of commissural de- and remyelination on motor skill behaviour in the cuprizone mouse model of multiple sclerosis. *Experimental Neurology*, *202*, 217–224.

Liu, L., Belkadi, A., Darnall, L., Hu, T., Drescher, C., Cotleur, A. C., Padovani-Claudio, D., He, T., Choi, K., Lane, T. E., Miller, R. H., & Ransohoff, R. M. (2010). CXCR2-positive neutrophils are essential for cuprizone-induced demyelination: Relevance to multiple sclerosis. *Nature Neuroscience*, *13*, 319–326.

Lubetzki, C., & Stankoff, B. (2014). Demyelination in multiple sclerosis. *Handbook of Clinical Neurology*, *122*, 89–99.

Lucchinetti, C., Brück, W., Parisi, J., Scheithauer, B., Rodriguez, M., & Lassmann, H. (2000). Heterogeneity of multiple sclerosis lesions: Implications for the pathogenesis of demyelination. *Annals of Neurology*, *47*, 707–717.

Ludwin, S. K. (1978). Central nervous system demyelination and remyelination in the mouse: An ultrastructural study of cuprizone toxicity. *Laboratory Investigation*, *39*, 597–612.

Mandwie, M., Karunia, J., Niaz, A., Keay, K. A., Musumeci, G., Rennie, C., McGrath, K., Al-Badri, G., & Castorina, A. (2021). Metformin treatment attenuates brain inflammation and rescues PACAP/VIP neuropeptide alterations in mice fed a high-fat diet. *International Journal of Molecular Sciences*, *22*, 13660.

Martin-Aguilar, L., Camps-Renom, P., Lleixa, C., Pascual-Goñi, E., Díaz-Manera, J., Rojas-García, R., De Luna, N., Gallardo, E., Cortés-Vicente, E., Muñoz, L., Alcolea, D., Lleó, A., Casasnovas, C., Homedes, C., Gutiérrez-Gutiérrez, G., Jimeno-Montero, M. C., Berciano, J., Sedano-Tous, M. J., García-Sobrino, T., … Querol, L. (2020). Serum neurofilament light chain predicts long-term prognosis in Guillain-Barre syndrome patients. *Journal of Neurology, Neurosurgery, and Psychiatry*, *5*, jnnp-2020-323899.

Matsushima, G. K., & Morell, P. (2001). The neurotoxicant, cuprizone, as a model to study demyelination and remyelination in the central nervous system. *Brain Pathology*, *11*, 107–116.

Mechelli, R., Annibali, V., Ristori, G., Vittori, D., Coarelli, G., & Salvetti, M. (2010). Multiple sclerosis etiology: Beyond genes and environment. *Expert Review of Clinical Immunology*, *6*, 481–490.

Metz, G. A., & Whishaw, I. Q. (2002). Cortical and subcortical lesions impair skilled walking in the ladder rung walking test: A new task to evaluate fore- and hindlimb stepping, placing, and co-ordination. *Journal of Neuroscience Methods*, *115*, 169–179.

Metz, G. A., & Whishaw, I. Q. (2009). The ladder rung walking task: A scoring system and its practical application. *Journal of Visualized Experiments*, *28*, 1204.

Mi, S., Blake Pepinsky, R., & Cadavid, D. (2013). Blocking LINGO-1 as a therapy to promote CNS repair: From concept to the clinic. *CNS Drugs*, *27*, 493–503.

Moro, O., Wakita, K., Ohnuma, M., Denda, S., Lerner, E. A., & Tajima, M. (1999). Functional characterization of structural alterations in the sequence of the vasodilatory peptide maxadilan yields a pituitary adenylate cyclase-activating peptide type 1 receptor-specific antagonist. *The Journal of Biological Chemistry*, *274*, 23103–23110.

Pennington, Z. T., Dong, Z., Feng, Y., Vetere, L. M., Page-Harley, L., Shuman, T., & Cai, D. J. (2019). ezTrack: An open-source video analysis pipeline for the investigation of animal behavior. *Scientific Reports*, *9*, 19979.

Piper, J. A., Al Hammouri, N., Jansen, M. I., Rodgers, K. J., Musumeci, G., Dhungana, A., Ghorbanpour, S. M., Bradfield, L. A., & Castorina, A. (2023). L-Proline prevents endoplasmic reticulum stress in microglial cells exposed to L-azetidine-2-carboxylic acid. *Molecules*, *28*, 4808.

Praet, J., Guglielmetti, C., Berneman, Z., Van der Linden, A., & Ponsaerts, P. (2014). Cellular and molecular neuropathology of the cuprizone mouse model: Clinical relevance for multiple sclerosis. *Neuroscience and Biobehavioral Reviews*, *47*, 485–505.

Prineas, J. W., & Parratt, J. D. (2012). Oligodendrocytes and the early multiple sclerosis lesion. *Annals of Neurology*, *72*, 18–31.

Ransohoff, R. M. (2012). Animal models of multiple sclerosis: The good, the bad and the bottom line. *Nature Neuroscience*, *15*, 1074–1077.

Scheuer, T., Endesfelder, S., Auf dem Brinke, E., Bührer, C., & Schmitz, T. (2022). Neonatal oxidative stress impairs cortical synapse formation and GABA homeostasis in Parvalbumin-expressing interneurons. *Oxidative Medicine and Cellular Longevity*, *2022*, 8469756.

Schildge, S., Bohrer, C., Beck, K., & Schachtrup, C. (2013). Isolation and culture of mouse cortical astrocytes. *Journal of Visualized Experiments*, *71*, 50079.

Seibenhener, M. L., & Wooten, M. C. (2015). Use of the open field maze to measure locomotor and anxiety-like behavior in mice. *Journal of Visualized Experiments*, *96*, e52434.

Slowik, A., Schmidt, T., Beyer, C., Amor, S., Clarner, T., & Kipp, M. (2015). The sphingosine 1-phosphate receptor agonist FTY720 is neuroprotective after cuprizone-induced CNS demyelination. *British Journal of Pharmacology*, *172*, 80–92.

Tan, Y. V., Abad, C., Lopez, R., Dong, H., Liu, S., Lee, A., Gomariz, R. P., Leceta, J., & Waschek, J. A. (2009). Pituitary adenylyl cyclase-activating polypeptide is an intrinsic regulator of Treg abundance and protects against experimental autoimmune encephalomyelitis.

Proceedings of the National Academy of Sciences of the United States of America, *106*, 2012–2017.

Tan, Y. V., Abad, C., Wang, Y., Lopez, R., & Waschek, J. (2015). VPAC2 (vasoactive intestinal peptide receptor type 2) receptor deficient mice develop exacerbated experimental autoimmune encephalomyelitis with increased Th1/Th17 and reduced Th2/Treg responses. *Brain, Behavior, and Immunity*, *44*, 167–175.

Tan, Y. V., Abad, C., Wang, Y., Lopez, R., & Waschek, J. A. (2013). Pituitary adenylate cyclase activating peptide deficient mice exhibit impaired thymic and extrathymic regulatory T cell proliferation during EAE. *PLoS One*, *8*, e61200.

Tan, Y. V., & Waschek, J. A. (2011). Targeting VIP and PACAP receptor signalling: New therapeutic strategies in multiple sclerosis. *ASN Neuro*, *3*, AN20110024.

Tatem, K. S., Quinn, J. L., Phadke, A., Yu, Q., Gordish-Dressman, H., & Nagaraju, K. (2014). Behavioral and locomotor measurements using an open field activity monitoring system for skeletal muscle diseases. *Journal of Visualized Experiments*, *91*, 51785.

Thomas Broome, S., Fisher, T., Faiz, A., Keay, K. A., Musumeci, G., Al-Badri, G., & Castorina, A. (2021). Assessing the anti-inflammatory activity of the anxiolytic drug buspirone using CRISPR-Cas9 gene editing in LPS-stimulated BV-2 microglial cells. *Cells*, *10*, 1312.

Trapp, B. D., & Nave, K. A. (2008). Multiple sclerosis: an immune or neurodegenerative disorder? *Annual Review of Neuroscience*, *31*, 247–269.

Tsiperson, V., Li, X., Schwartz, G. J., Raine, C. S., & Shafit-Zagardo, B. (2010). GAS6 enhances repair following cuprizone-induced demyelination. *PLoS One*, *5*, e15748.

van den Bosch, A., Fransen, N., Mason, M., Rozemuller, A. J., Teunissen, C., Smolders, J., & Huitinga, I. (2022). Neurofilament light chain levels in multiple sclerosis correlate with lesions containing foamy macrophages and with acute axonal damage. *Neurology Neuroimmunology & Neuroinflammation*, *9*, e1154.

Vincze, A., Reglodi, D., Helyes, Z., Hashimoto, H., Shintani, N., & Abraham, H. (2011). Role of endogenous pituitary adenylate cyclase activating polypeptide (PACAP) in myelination of the rodent brain: Lessons from PACAP-deficient mice. *International Journal of Developmental Neuroscience*, *29*, 923–935.

Wagenknecht, N., Becker, B., Scheld, M., Beyer, C., Clarner, T., Hochstrasser, T., & Kipp, M. (2016). Thalamus degeneration and inflammation in two distinct multiple sclerosis animal models. *Journal of Molecular Neuroscience*, *60*, 102–114.

Walker, D. G., & Lue, L. F. (2015). Immune phenotypes of microglia in human neurodegenerative disease: Challenges to detecting microglial polarization in human brains. *Alzheimer's Research & Therapy*, *7*, 56.

Wang, H., Li, C., Wang, H., Mei, F., Liu, Z., Shen, H. Y., & Xiao, L. (2013). Cuprizone-induced demyelination in mice: Age-related vulnerability and exploratory behavior deficit. *Neuroscience Bulletin*, *29*, 251–259.

Waschek, J. A. (2013). VIP and PACAP: Neuropeptide modulators of CNS inflammation, injury, and repair. *British Journal of Pharmacology*, *169*, 512–523.

Wegener, A., Deboux, C., Bachelin, C., Frah, M., Kerninon, C., Seilhean, D., Weider, M., Wegner, M., & Nait-Oumesmar, B. (2015). Gain of Olig2 function in oligodendrocyte progenitors promotes remyelination. *Brain*, *138*, 120–135.

Yamanaka, K., Nakamura, K., Shibahara, T., Takashima, M., Takaki, H., Hidaka, M., Komori, M., Yoshikawa, Y., Wakisaka, Y., Ago, T., & Kitazono, T. (2023). Deletion of Nox4 enhances remyelination following cuprizone-induced demyelination by increasing phagocytic capacity of microglia and macrophages in mice. *Glia*, *71*, 541–559.

Yang, Z., & Wang, K. K. (2015). Glial fibrillary acidic protein: From intermediate filament assembly and gliosis to neurobiomarker. *Trends in Neurosciences*, *38*, 364–374.

Ye, J. N., Chen, X. S., Su, L., Liu, Y. L., Cai, Q. Y., Zhan, X. L., Xu, Y., Zhao, S. F., & Yao, Z. X. (2013). Progesterone alleviates neural behavioral deficits and demyelination with reduced degeneration of oligodendroglial cells in cuprizone-induced mice. *PLoS One*, *8*, e54590.

Zhang, Y., Cai, L., Fan, K., Fan, B., Li, N., Gao, W., Yang, X., & Ma, J. (2019). The spatial and temporal characters of demyelination and remyelination in the cuprizone animal model. *The Anatomical Record*, *302*, 2020–2029.

Zhou, Q., Wang, S., & Anderson, D. J. (2000). Identification of a novel family of oligodendrocyte lineage-specific basic helix-loop-helix transcription factors. *Neuron*, *25*, 331–343.

SUPPORTING INFORMATION

Additional supporting information can be found online in the Supporting Information section at the end of this article.

How to cite this article: Jansen, M. I., Mahmood, Y., Lee, J., Broome, S. T., Waschek, J. A., & Castorina, A. (2024). Targeting the PAC1 receptor mitigates degradation of myelin and synaptic markers and diminishes locomotor deficits in the cuprizone demyelination model. *Journal of Neurochemistry*, *168*, 3250–3267. https://doi.org/10.1111/jnc.16199